Selectivity and Permeation in Calcium Release Channel of Cardiac Muscle: Alkali Metal Ions

Duan P. Chen,* Le Xu,# Ashutosh Tripathy,# Gerhard Meissner,# and Bob Eisenberg*
*Department of Molecular Biophysics and Physiology, Rush Medical College, Chicago, Illinois 60612, and #Department of Biochemistry and Biophysics, University of North Carolina, Chapel Hill, North Carolina 27599 USA

ABSTRACT Current was measured from single open channels of the calcium release channel (CRC) of cardiac sarcoplasmic reticulum (over the range ±180 mV) in pure and mixed solutions (e.g., biionic conditions) of the alkali metal ions Li^+, K^+, Na^+, Rb^+, Cs^+, ranging in concentration from 25 mM to 2 M. The current-voltage (*I-V*) relations were analyzed by an extension of the Poisson-Nernst-Planck (PNP) formulation of electrodiffusion, which includes local chemical interaction described by an offset in chemical potential, which likely reflects the difference in dehydration/solvation/rehydration energies in the entry/exit steps of permeation. The theory fits all of the data with few adjustable parameters: the diffusion coefficient of each ion species, the average effective charge distribution on the wall of the pore, and an offset in chemical potential for lithium and sodium ions. In particular, the theory explains the discrepancy between "selectivities" defined by conductance sequence and "selectivities" determined by the permeability ratios (i.e., reversal potentials) in biionic conditions. The extended PNP formulation seems to offer a successful combined treatment of selectivity and permeation. Conductance selectivity in this channel arises mostly from friction: different species of ions have different diffusion coefficients in the channel. Permeability selectivity of an ion is determined by its electrochemical potential gradient and local chemical interaction with the channel. Neither selectivity (in CRC) seems to involve different electrostatic interaction of different ions with the channel protein, even though the ions have widely varying diameters.

INTRODUCTION

Selectivity and permeation are inseparable functions of ionic channels, and they demand a combined treatment, because selectivity reveals itself only through permeation. Selectivity is evaluated experimentally in two ways, either from the ratio of ionic conductances or from the ratio of permeabilities estimated from reversal potentials by constant field theory (Eisenman and Horn, 1983). The reversal potential is the membrane holding potential at which the current-voltage relation changes its sign, and the conductance is the slope of the current-voltage relation. In the constant field theory of Goldman, Hodgkin, and Katz (GHK) (Goldman, 1943; Hodgkin and Katz, 1949), selectivity arises from the friction between ions and "the membrane." Different types of ions experience different amounts of friction and so have different diffusion coefficients. In the constant field theory, permeability is defined as the diffusion coefficient divided by the channel length (the partition coefficient is set at 1). That is its physical meaning. The value of the diffusion coefficient or permeability is estimated experimentally from the reversal potential.

Electrostatics plays a central role in biology (Parsegian, 1969; Honig and Nichols, 1995; Davis and McCammon, 1990; Jordan, 1982; Forsten et al., 1994), and ionic channels are no exception. Electrostatic interactions between channel protein and ion are likely to be involved in ion movement, although they are ignored in the GHK theory. Indeed, Eisenman (Eisenman, 1962; Simon and Morf, 1973; Reuter and Stevens, 1981) describes conductance selectivity entirely as an electrostatic phenomenon, arising from a binding competition between the dehydration and attraction of ions to a channel pore; selectivity is produced by equilibrium binding in Eisenman's theory.

Conductance selectivity achieved by binding has been seen as paradoxical for a long time (Bezanilla and Armstrong, 1972; Neyton and Miller, 1988), particularly when the affinity of binding is high. How can a tightly held ion have the same friction or freedom of motion (i.e., entropy) as a weakly held ion? We shall see that this paradox does not arise in a PNP-based treatment.

The calcium release channel (CRC) of the sarcoplasmic reticulum (SR) is a high-conductance channel that selects cations over anions and divalent cations over monovalent cations. Potassium ions permeate CRC with a conductance of 800 pS when bathed in 250 mM symmetrical KCl solutions (i.e., 250 mM‖250 mM). The "permeability ratio" for potassium/chloride is nearly 20 (Williams, 1992; Lindsay et al., 1991; Chen et al., 1997b), from the conventional estimate of the ratio, determined from reversal potentials by the GHK equation (Hille, 1992, equation 1-13, and see our Eq. 12).

The CRC of the SR plays a central role in the activation of contraction, and it is permeable to the monovalent cations Li^+, K^+, Na^+, Rb^+, and Cs^+. The structure of the CRC consists of four polypeptides; each consists of ~5000 amino acid residues (Meissner, 1994). CRC and related calcium channels have been studied extensively by electrophysiolo-

Received for publication 19 June 1998 and in final form 30 October 1998.
Address reprint requests to Dr. Duan P. Chen, Department of Molecular Biophysics and Physiology, Rush Medical College, 1750 Harrison St., JS1298, Chicago, IL 60612-3824. Tel.: 312-942-5312; Fax: 312-942-8711; E-mail: dchen@rush.edu; Web site: http://144.74.27.66/reprint.html.

0006-3495/99/03/1346/21 $2.00

gists (Coronado et al., 1994; Meissner, 1994) and molecular biologists (Asther et al., 1994). We have shown that the movement of K^+ through the CRC channel is easily understood by the Poisson-Nernst-Planck (PNP) formulation (Chen et al., 1997b). Channel models (Williams, 1992), using the traditional formulation of Eyring rate theory (Hille and Schwarz, 1978), do not fit the data in asymmetrical solutions and have difficulty fitting the data at high membrane potential. These models ignore many effects that concern other scientists studying ionic movement in condensed matter (Hänggi et al., 1990).

Measuring selectivity always involves measurements of fluxes (whether selectivity is measured by conductance or permeability ratio), because there is even current flow at the reversal potential. Thus a kinetic model of selectivity is needed that predicts flux from the effects of equilibrium binding. In Eisenman's theory, Eyring rate theory was used (Hille and Schwarz, 1978). Within the channel's pore, different ions were supposed to have different chemical interactions described by different profiles of free energy (Hille, 1975). Entropy differences between ions in the bath and channel were ignored (Berry et al., 1980, pp. 1147–1165) along with friction; kT/h was used as the prefactor in the rate expressions. Our goal is to see how well another kinetic model—the PNP formulation—can explain the selectivity and permeation of CRC.

MATERIALS AND METHODS

Single-channel measurements were made by reconstituting purified cardiac muscle CRC into Mueller-Rudin-type bilayers (of phosphatidylethanolamine, phosphatidylserine, and phosphatidylcholine in 5:3:2 composition). We add the purified channel proteins to the *cis* side, while the other side (*trans*) is electrically grounded. The solutions contain 2 mM KHEPES at pH 7.5 with 4 μM Ca^{2+}, in addition to the salts listed in Table 1. Data are sampled at 10 kHz, filtered at 2 kHz, and analyzed by pClamp software by Axon Instruments.

We analyze the permeation data of monovalent cations (Li^+, Na^+, K^+, Rb^+, and Cs^+) through the CRC by the PNP formulation of electrodiffusion (Chen and Eisenberg, 1993a) and its extension to include local chemical interaction (Chen, 1997; Nonner et al., 1998).

To solve the coupled Poisson-Nernst-Planck equations, we have analyzed the coupled Poisson-Nernst-Planck electrodiffusion equations for a cylindrical pore in the lipid membrane by both the singular perturbation technique (Barcilon et al., 1992) and cross-sectional averaging (Chen and Eisenberg, 1992), and we have shown that the following are the leading order equations:

$$-\epsilon_a \Psi''(z) = \frac{2\epsilon_m}{a^2 \ln a/d}[(1 - z/d)\Delta + \Psi(z) - \Psi_{bi}(d)] + \sum_j z_j e C_j(z) + P(z), \tag{1}$$

$$J_j = -D_j\left[\frac{dC_j(z)}{dz} + z_j\frac{e}{k_B T}C_j(z)\frac{d\Psi(z)}{dz} + \frac{C_j(z)}{k_B T}\frac{d\bar{\mu}_j}{dz}\right], \quad \text{for } j = 1, \ldots, N, \tag{2}$$

with boundary conditions

$$\Psi(0) = \Psi_{bi}(0) + V_{appl}, \tag{3}$$

$$\Psi(d) = \Psi_{bi}(d), \tag{4}$$

$$C_j(0) = C_j(L)e^{-z_j e\Psi_{bi}(0)/k_B T}, \quad \text{for } j = 1, \ldots, N, \text{ at } z = 0, \tag{5}$$

$$C_j(d) = C_j(R)e^{-z_j e\Psi_{bi}(d)/k_B T}, \quad \text{for } j = 1, \ldots, N, \text{ at } z = d, \tag{6}$$

where d is the length of the channel, a is the radius, $P(z)$ is the charge distribution of the channel protein defined in the domain $[0, d]$, $C_j(L)$ is the

TABLE 1 The list of 40 solutions of alkaline metal chlorides, at which current-voltage relations are measured

Salt	Concentrations (*cis*‖*trans*) (in mM)					
LiCl	250‖250	250‖25	250‖1000	1000‖100		
NaCl	250‖250	250‖25	1000‖1000	1000‖100	1000‖500	
KCl	250‖250	250‖25	1000‖1000	1000‖100	250‖50	250‖100
	250‖500	250‖1000	1000‖250	1000‖500	250‖2000	2000‖100
RbCl	250‖250	250‖25	1000‖1000	1000‖100		
CsCl	250‖250	250‖25	1000‖1000	1000‖100	1000‖500	
	Biionic solutions (*cis*‖*trans*) (in mM)					
KCl‖LiCl	250‖250	500‖500	1000‖1000	250‖50		
KCl‖NaCl	250‖250					
KCl‖RbCl	250‖250					
KCl‖CsCl	250‖250					
	KCl and LiCl mole-fraction experiments at a total of 250 mM (symmetrical *trans* and *cis*)					
10% KCl	25 mM KCl & 225 mM LiCl					
50% KCl	125 mM KCl & 125 mM LiCl					
90% KCl	225 mM KCl & 25 mM LiCl					

There are four solutions for LiCl, five for NaCl, 12 for KCl, four for RbCl, and five for CsCl. There are mole fraction experiments and experiments in biionic solutions. The total number of *I-V* points is 1203, with a root mean square of 55 pA.

concentration in the left bath; $C_j(R)$ is the concentration in the right bath; ϵ_a is the dielectric constant of the aqueous pore; ϵ_m is the dielectric constant of the channel protein; V_{appl} is the applied voltage; $\Delta = V_{appl} + \Psi_{bi}(0) - \Psi_{bi}(d)$; and Ψ_{bi} is the usual Donnan potential (Chen and Eisenberg, 1993a; Selberherr, 1984; Green and Andersen, 1991). $\bar{\mu}_j$ is the "excess" chemical potential discussed later; the subscript j denotes the ion species. The electric current is then $I = A\Sigma_j e z_j J_j$, where A is the channel cross-sectional area.

The first term on the right-hand side of the above modified Poisson equation is a dielectric polarization charge. The second term is the charge carried by the mobile ions, and the third term is the charge on the channel protein (see Eq. 1). The first term in the ion flux formula (see Eq. 2) is driven by the concentration gradient, which is due to thermal motion and is an effect of entropy production (Chen and Eisenberg, 1993b, Appendix). The second term in the flux formula is electrically driven, and the third is from the gradient of chemical potential due to different local chemical interaction.

To use the Nernst-Planck equation (Eq. 2), we need to know the electric field; the electric field is determined, however, by the Poisson equation (see Eq. 1). Therefore, to calculate the ion flux, we need to solve the Nernst-Planck equation and the Poisson equation together.

The "excess" chemical potential ($\bar{\mu}_j$) for ion species j adds to the electrical and concentration terms of the free energy (per mole) to give the total free energy per mole (i.e., the electrochemical potential),

$$\mu_j = k_B T \ln C_j + z_j e\Psi + \bar{\mu}_j.$$

The excess chemical potential represents the free energy needed for an ion to occupy a space in the restricted special environment of the channel's pore, in addition to the usual electrical energy and entropic energy due to concentration. It includes all energy and entropy terms that are not described by simple concentration and (mean) electric field terms, e.g., van der Waals energies and internal polarization energies (both of which are usually classified as part of the energy of chemical interaction). It can also contain terms arising from the dehydration of ions from water and their subsequent resolvation by the channel protein.

If considered a description of localized chemical interaction, the excess chemical potential ($\bar{\mu}_j$) would be expected to vary strongly with position, and its variation could drive a third chemically specific component of ion flux (see Eq. 2): it could provide selectivity among ions of the same valence and concentration. However, certain thermodynamic difficulties arise in that case, because the source of energy of gradients in $\bar{\mu}_j$ must then be included in the entire analysis. Otherwise, flux can arise without an external source of free energy. These problems do not arise here because $\bar{\mu}_j$ is spatially uniform in our analysis: it is an offset from the bulk value of the electrochemical potential. In the next section of the paper, we show how the gradients at the ends of the channel can be handled.

The coupled Poisson and Nernst-Planck equations are solved numerically by iteration. An initial guess of electrical potential is used to compute a congruent initial guess of the ion concentration profiles by Eq. 2. Then that concentration profile is substituted into Eq. 1 to update the profile of the electrical potential to a second, more refined approximation. This procedure is iterated until successive iterations give the same answer within a convergence tolerance.

The integration of the Nernst-Planck equations can be done analytically for one-dimensional systems. The Poisson equation is solved numerically using this analytical result and an exponential fitting of the Poisson equation (the code is available at http://144.74.27.66/pnp.html, and the details are discussed in Chen and Eisenberg, 1993b). Least-squares fits were determined by a modified Levenburg-Marquardt procedure (Press et al., 1992), and the singular value decomposition was used to test the dependencies of the least-squares parameters (Van Huffel and Vandewalle, 1991).

The quality of a least-squares fit was measured by the ratio of the rms value of the error to the rms value of the actual current I, because the error at each I-V point measurement is difficult to obtain experimentally (otherwise, we would use the standard χ^2 test). The rms value of the actual current I is defined as

$$I_{rms} = \sqrt{\frac{1}{N}\sum_i \sum_j I_{ij}^2}, \tag{7}$$

where N is the total number of I-V points in all measured current-voltage relations of all solutions, i denotes the ionic solution, j denotes the I-V points in the measured current-voltage relation of the same ionic solution, and I_{ij} is the value of the jth measured electrical current in the ith ionic solution. The rms value of errors of the least-squares fit is defined as

$$\delta_{rms} = \sqrt{\frac{1}{N}\sum_i \sum_j (I_{ij}^{PNP} - I_{ij})^2}, \tag{8}$$

where I_{ij}^{PNP} denotes the electrical current calculated by PNP. Another measure of deviation or goodness of the fit is a scaled rms defined as

$$\delta_{rms}^{scaled} = \sqrt{\frac{1}{N}\sum_i \frac{1}{I_{i,max}^2} \sum_j (I_{ij}^{PNP} - I_{ij})^2}, \tag{9}$$

where $I_{i,max}$ is the maximum absolute electric current magnitude within the current-voltage relation of the i-solution.

RESULTS

Homogeneous solutions

In this section, we see how much of selectivity and permeation is explained by electrostatic interactions only. In other words, we consider the Eisenman hypothesis that selectivity is produced only by the difference in electrostatic binding energy of different ions to the channel protein. Therefore, in this section, chemical interaction is ignored by setting $\bar{\mu}_j$ to zero, and we consider mostly measurements in ionic solutions of one salt, like the symmetrical 250 mM‖250 mM KCl or the asymmetrical 250 mM‖25 mM RbCl. The channel's filter region is set at a length of 10 Å (Tu et al., 1994; Tinker and Williams, 1995) and a diameter of 7 Å (Meissner, 1986; Smith et al., 1988). The dielectric constant for protein and lipid (ϵ_m) is chosen to be 5, and for water ϵ_a = 80 (see discussion later). We have performed a constrained least-squares fit to use our experimental information maximally, assuming that the charge distribution of the CRC pore and the diffusion coefficient of chloride ions are the same at all transmembrane voltages in all different salt solutions of LiCl, NaCl, KCl, RbCl, and CsCl. The parameters estimated by the least-squares procedure are D(Li), D(Na), D(K), D(Rb), D(Cs), D(Cl), and $P(z)$, which is assumed to be independent of z. The charge distribution of the channel is assumed to be spatially uniform and so is described by a single number for all potentials, types, and concentrations of ions (Chen et al., 1997b). The ionic "concentrations" C_j are the activities listed by Robinson and Stokes (1959).

We have separately reported the fit of PNP to the 12 I-V's for KCl, which gave parameter estimates $P(z) = -4.18$ M, $D(K) = 1.25 \times 10^{-6}$, D(Cl) $= 3.87 \times 10^{-6}$ cm^2/s (Chen et al., 1997b). These estimates (together with $\bar{\mu}$(K) = $\bar{\mu}$(Cl) =

0) form the initial guess for the present curve-fitting calculations. The resulting estimates of parameters from all data in LiCl, NaCl, KCl, RbCl, and CsCl are $D(\mathrm{Li}) = 3.20 \times 10^{-7}$, $D(\mathrm{Na}) = 7.83 \times 10^{-7}$, $D(\mathrm{K}) = 1.27 \times 10^{-6}$, $D(\mathrm{Rb}) = 1.11 \times 10^{-6}$, $D(\mathrm{Cs}) = 8.30 \times 10^{-7}$, $D(\mathrm{Cl}) = 4.02 \times 10^{-6}$ cm^2/s, and $P(z) = -4.38$ M.

The total fixed charge is nearly one elementary charge. That is to say, $\pi r^2 \int P(z)\mathrm{d}z = -1.02e$. The values of $D(\mathrm{K})$, $D(\mathrm{Cl})$, and $P(z)$ are within 5% of those obtained by fitting the KCl data alone (Chen et al., 1997b). We have also fitted by setting $\epsilon_m = 10$, and get a similar result.

The δ_{rms} (defined in Eq. 8) of the fit is 4.5 pA, which is 8% of the rms current size (I_{rms} defined in Eq. 7) of 57 pA. In general, there is a quite good agreement between the experiment and the calculation (see Figs. 2–5). (Deviations at large voltages are not surprising (see Chen et al., 1997b).)

Again, in this section, we investigate the electrostatic contribution to the permeation of CRC and set $\bar{\mu}_j = 0$ for all ion species. Fig. 1 shows a typical experimental single-channel recording of CRC bathed in 250 mM‖25 mM LiCl solution at various holding membrane potentials. Fig. 2 shows the worst fits among all salt solutions, which are the four LiCl *I-V*'s. The lines are the theoretical curves from PNP with $\bar{\mu}_j = 0$. The symbols are the experimental points, which also label the ionic solutions. There is some significant misfit in 1 M‖100 mM and 250 mM‖1 M solutions, and that misfit is the major source of error in the entire fit to all curves of all salts. The fits to the Li^+ data are poor enough to require changes in the theory: in the next section of the Results we add a chemical term $\bar{\mu}_j$ to the free energy and improve the fits dramatically (see Fig. 10).

Figs. 3–5 show the fits to the five NaCl current-voltage relations, four RbCl *I-V*'s, and five CsCl current-voltage relations. The fit to the 12 KCl *I-V*'s is almost identical to that reported in Chen et al. (1997b); hence it is omitted.

The fits are excellent except in 250 mM‖25 mM solutions, where we have found a change in slope conductance near the reversal potential. We are planning to investigate this slope conductance change further.

Fig. 6 shows the relation between the measured ionic conductance and estimates of diffusion coefficients. The conductance normalized by the conductance for K^+ is plot-

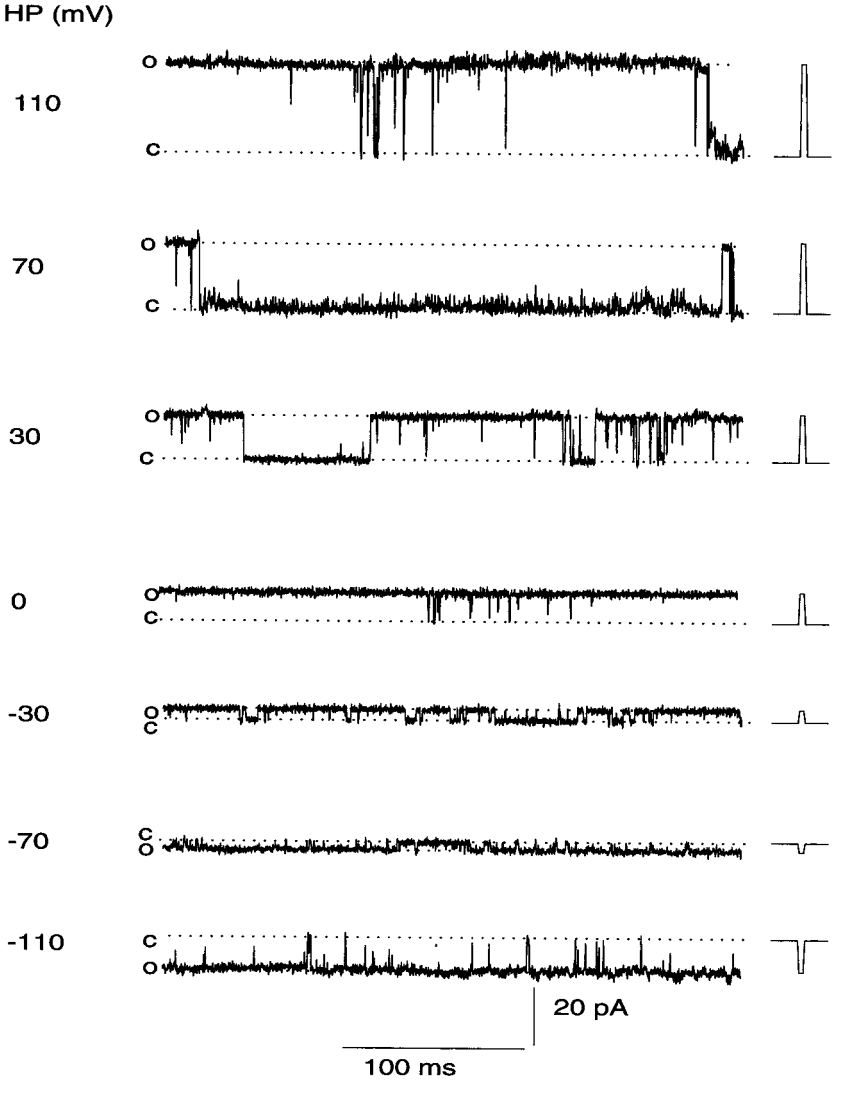

FIGURE 1 The typical single-channel recording of CRC channels bathed in 250 mM‖25 mM LiCl solution is shown at different membrane holding potentials. The numbers on the left-hand side indicate the holding potentials. The traces on the right-hand side show the direction of openings and the current magnitude of PNP predictions. In the single-channel analysis, the partial openings in the experimental record are deleted to give an average open magnitude. The current and time scale are shown at the bottom of the graph.

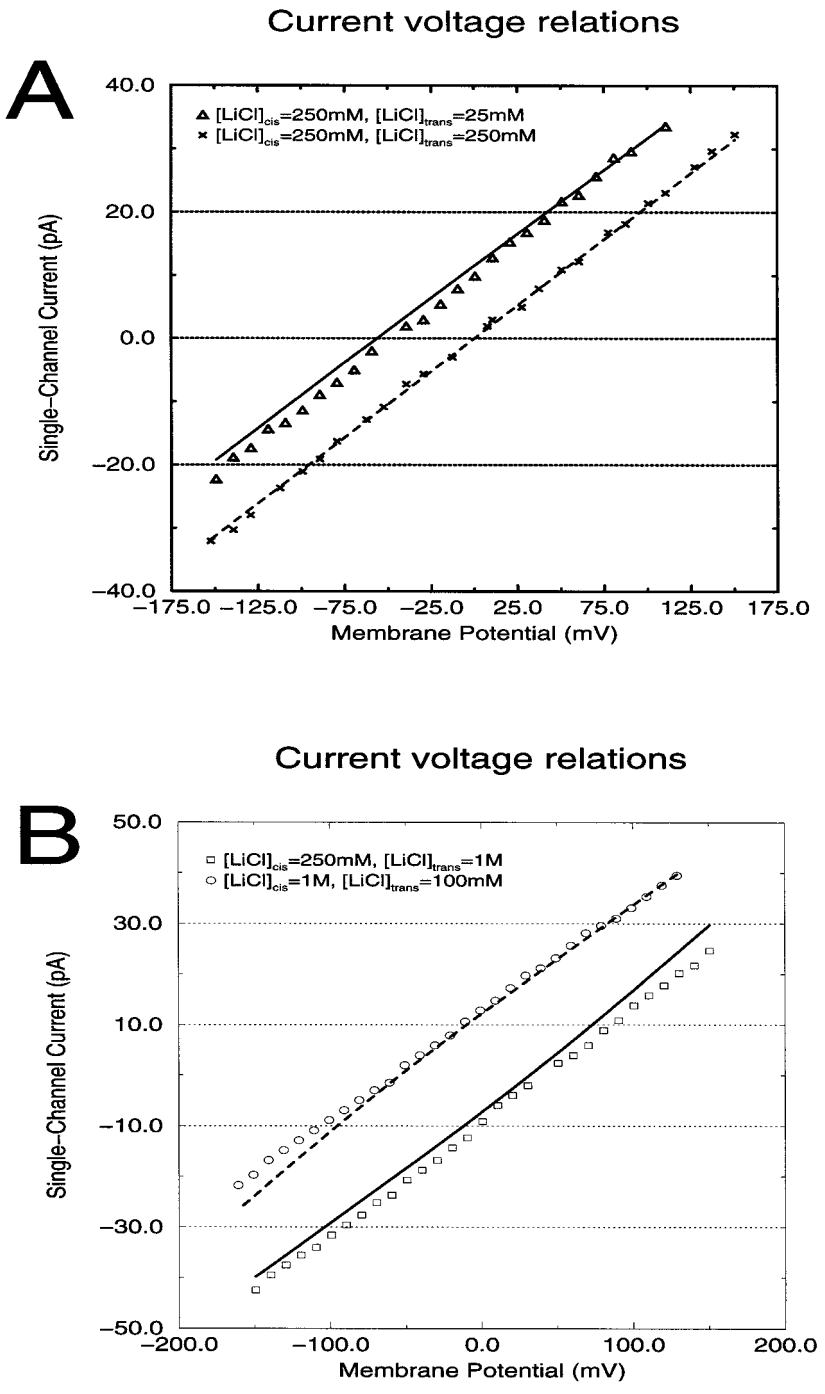

FIGURE 2 The current-voltage relations for LiCl are fitted simultaneously with *I-V*'s of NaCl, KCl, RbCl, and CsCl. The symbols show the experiment, and the lines are the fits of PNP. The salt solution is indicated in the legend next to the experimental symbols. There are four *I-V*'s for LiCl. We consider the lower panel poor fits, but they are later corrected in Fig. 11.

ted against estimates D_j of the diffusion coefficients of ions in the channel normalized by D_K. The square symbols are experimental points, and the solid line is obtained by a linear least-square fit to those points. The line is of slope 0.995 with a standard deviation of 0.029 and has an intercept of 0.02 with a standard deviation of 0.02. Clearly, the line goes through the origin with a slope of 1, within the errors indicated. This result shows that estimates of diffusion coefficients are entirely determined by the measured conductance. In other words, the conductance selectivity of CRC as estimated by its slope conductance is entirely an effect of the diffusion coefficients. No other property of the channel seems to determine the slope conductance of this channel in these solutions. The electrical energy does not seem to be involved explicitly in determining the selectivity of alkali metal ions.

All permeating ion species interact with the same profile of electrical potential in the PNP model, and thus all ion species of the same charge (i.e., valence) have the same electrical energy despite their differences in diameter. The concentration profile of each ion can be computed directly from the potential profile, given the bath concentrations and

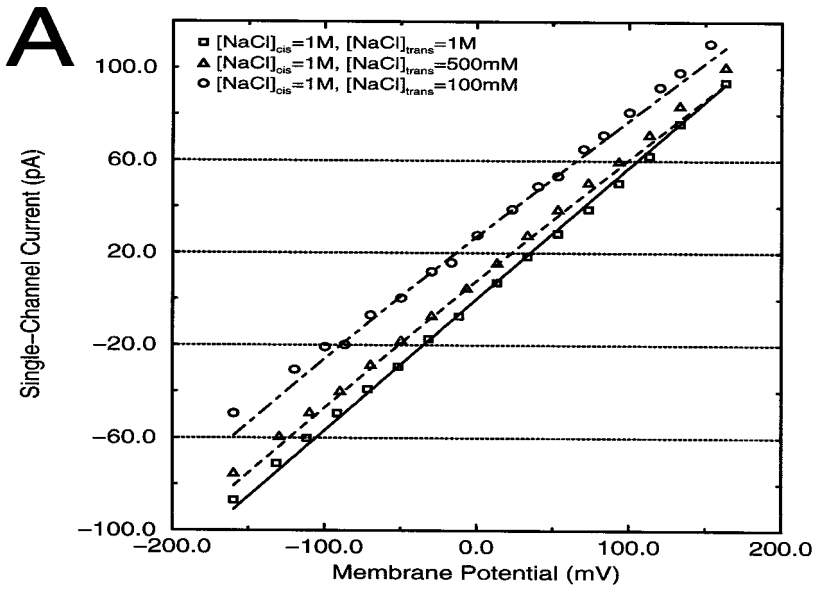

FIGURE 3 The fits to the five current-voltage relations of NaCl. The conventions are the same as those in Fig. 1.

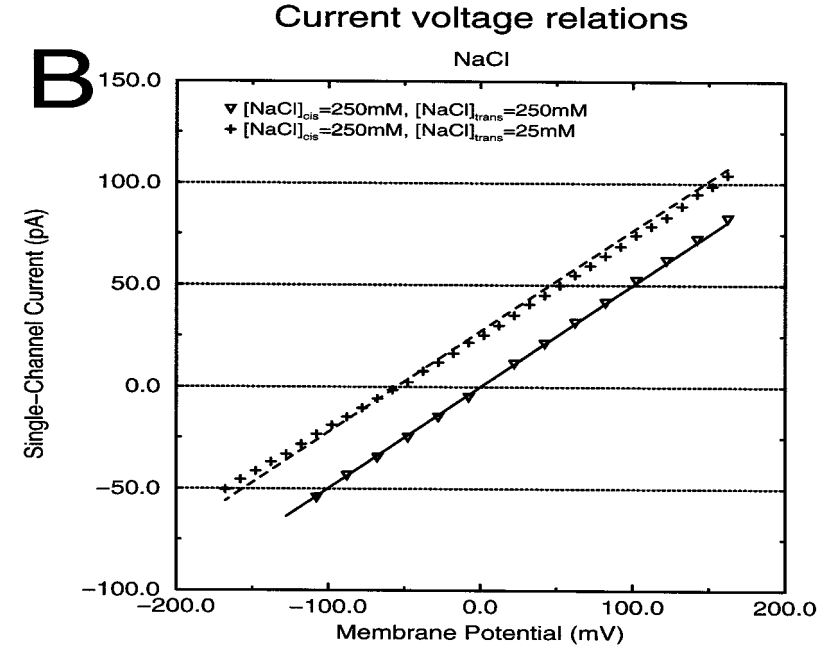

valence of the ion. No other parameters are involved (see, for example, equation 9 of Chen et al., 1997a). Thus the spatial distribution of concentration of all ions is the same, if they are held at the same bath concentrations.

Fig. 7 *A* shows that the content of the pore is highly buffered, even in different ionic solutions. In Fig. 7 *A*, the concentration profiles of potassium ions are shown for asymmetrical 250:25 mM, symmetrical salts of 250 mM, and symmetrical 1 M KCl solutions at the applied transmembrane potential of 100 mV. We omit the portion of the profiles in the baths, and we omit entirely the concentration profiles of chloride ions, because they are so small that they barely affect the conductance (they are similar to what is reported by Chen et al., 1997b). The solid line is the profile for the solution of 250:25 mM, the dashed line is for 250 mM symmetrical salt, and the long-dashed line is for symmetrical 1 M KCl. They nearly overlap, considering the extended scale used in the graph. The occupancy of potassium ions is given by the integral

$$O_{K^+} = \pi r^2 N_A \int_o^d C(K^+, \zeta) d\zeta, \qquad (10)$$

where N_A is Avogadro's number, and d is the length of the channel. The calculated occupancies are 1.0154, 1.0164,

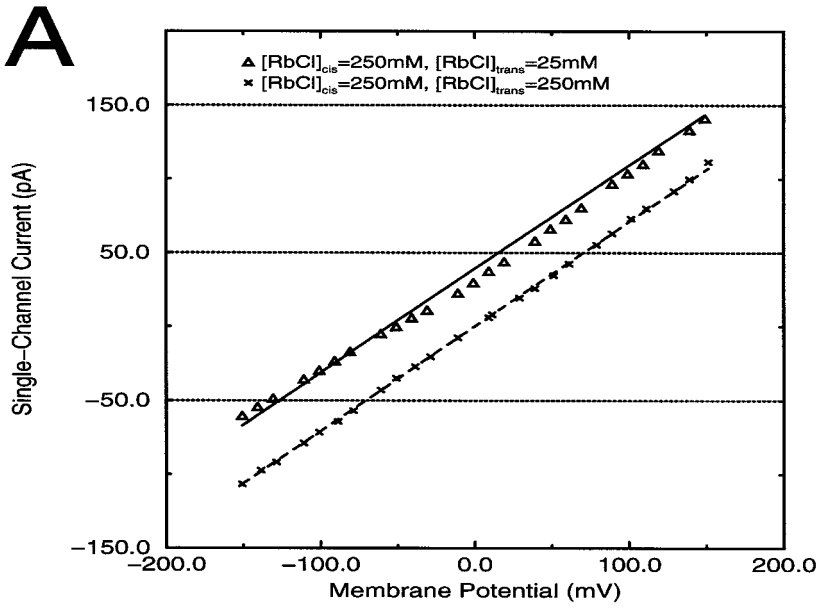

FIGURE 4 The fits to the four current-voltage relations of RbCl. The conventions are the same as those used in Fig. 1.

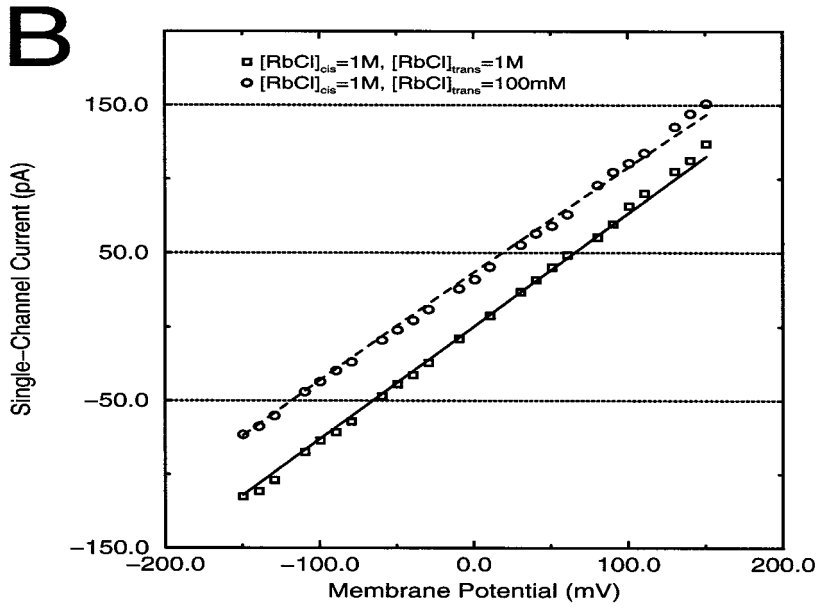

and 1.0337, respectively, for the above three solutions. The occupancies barely change from solution to solution, and the content of the pore is highly buffered.

Table 2 summarizes the conductance, the reversal potential, and the occupancy of potassium ions in the above three salt solutions. The slope conductance in Table 3 is calculated by $\gamma = (I(V = 100)/(100 - V_{rev})$. From asymmetrical 250‖25 mM to symmetrical salts of 250 mM, the occupancy of potassium ion is nearly the same, and so is the conductance (795 pS versus 791 pS). What changes is the net driving force, and such change shifts the reversal potential to −48 mV in the asymmetrical 250:25 mM solution. From symmetrical 250 mM to symmetrical 1 M solution, the occupancy of potassium ions again remains nearly the same. The change in potassium ion occupancy is less than 2% from 1.0164 to 1.0337. The conductance of the permeating potassium ions, however, changes significantly, but not as much as the increase in ionic strength, from 791 pS of 250‖250 mM to 933 pS of 1 M‖1 M, even though the occupancies of potassium ions are nearly the same. If the channel's pore is such a buffered system, it is natural to wonder why its conductance varies at all.

What really makes a difference in conductance is the combination of the direct effect of change in concentration

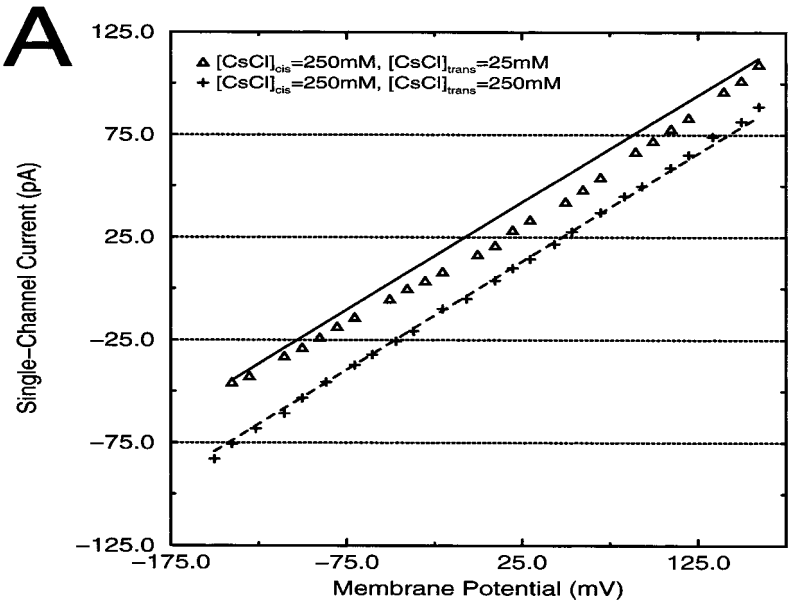

FIGURE 5 The fits to the five current-voltage relations of CsCl. The conventions are the same as those used in Fig. 1. We have a poor fit for 250 mM‖25 mM solution.

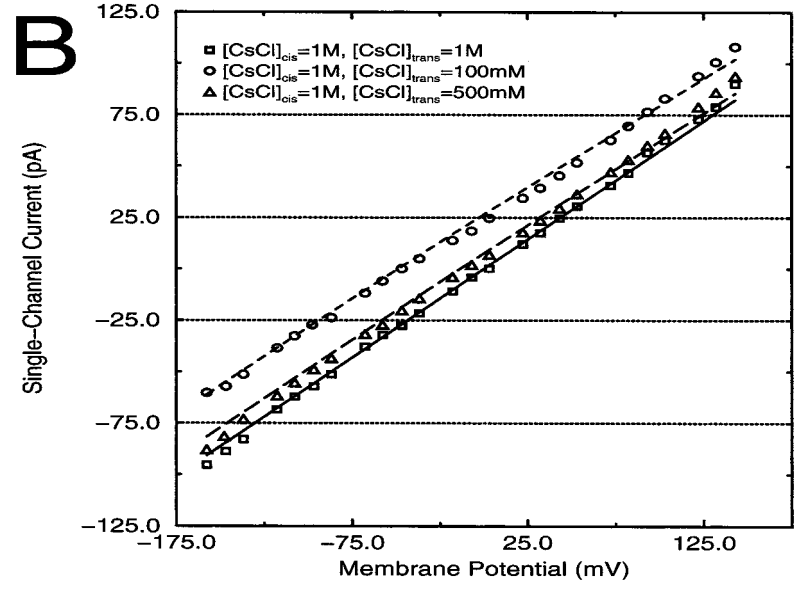

and the electrostatic screening of surface charge at the entrances of the channel.

Fig. 7 *B* shows the electrical potential profiles for the above three ionic solutions, where the solid line is for 250:25 mM, the dashed line is for 250 mM symmetrical salt, and the long-dashed line is for symmetrical 1 M KCl. From 250:25 mM to symmetrical 250 mM solution, there is a large difference in the *trans* bath potential due to ionic strength-dependent screening. Consequently, the net voltage drop is very different in the two cases—that is what makes different reversal potentials, but nearly the same slope conductances.

From 250 mM to 1 M symmetrical solutions, the ionic strength is increased by a factor of 3.4 (ratio of activities at 1 M and 250 mM, 0.6040/0.1754), but conductance is changed 18% from 791 pS to 933 pS. Comparing these two ionic solutions, the screening of the surface charge in the two baths is rather different, having a quite opposite effect. The potential in the 1 M solution is 30.25 mV higher than that in the 250 mM solution. This shift is caused by the change in electrostatic screening of the negatively charged surface charge at the entrances of the channel when the bath is changed. A shift in the electrical potential of 30.25 mV is 1.2 k_BT, which is a factor of $e^{1.21} = 3.35$ in favor of the 250

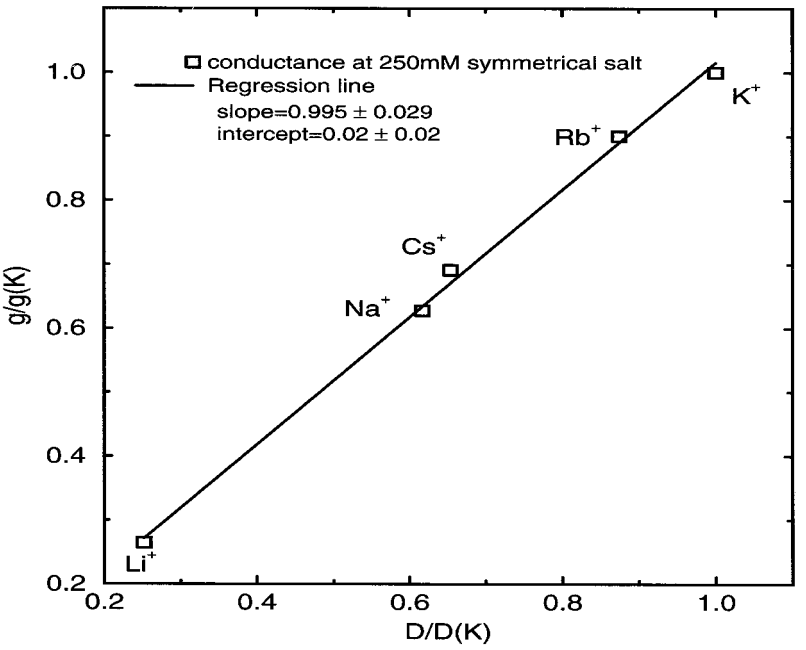

FIGURE 6 The ratios of conductances at 250 mM symmetrical salts are plotted against the ratios of diffusion coefficients. Different salts are labeled by their chemical symbol of the main permeating cation. The line is drawn by a linear regression through the above points. The linear regression gives a line through the origin of slope 1, showing the strong correlation between the measured conductance and the estimated diffusion coefficients.

mM solution. The combined effect of the increase in ionic strength and the increase in the electrostatic screening makes the slope conductance saturate.

In summary, the ionic occupancies in an open channel are nearly constant from solution to solution for a wide range of electrical potentials. What governs the ionic conductance of an open channel is the electrical potential and effects of screening of the electrical potential, along with the direct effect of bath concentration.

We have tested the possibility that the measured selectivity among alkali metal ions for CRC is caused by the different electrostatic interaction of different alkali ions with the channel wall. We made a different least-squares fit by setting all of the diffusion coefficients of the alkali cations to the same value, but allowing different ions to see a different charge distribution of the CRC pore. If electrostatics alone could account for selectivity, i.e., for the measurements of *I-V* curves in this range of homogeneous solutions, it would be seen this way as different profiles of fixed charge for each ion. However, this procedure does not give a reasonable fit of the measured data. The best fit gives a δ_{rms} of 8.4 pA (nearly double the error reported earlier, $\delta_{rms} = 4.5$), if all diffusion coefficients of alkali ions are the same. This fit misses altogether most of the current-voltage relations measured in asymmetrical salt solutions. This finding suggests that the diffusion coefficients for different alkali ions must be different, regardless of whether the charge distribution is altered when different ions occupy the CRC pore. This finding shows that if the friction (diffusion coefficient) is the same for all alkali metal cations, the electrostatic interaction alone cannot explain the selectivity of CRC.

The electrodiffusion description apparently captures the main features of CRC permeation in solutions of one salt, NaCl, KCl, RbCl, or CsCl. This result is really quite surprising, given the evident difference between these ions, seen in their atomic properties (for example, their different ionic radii, electronic structure, and different hydration energies) or their macroscopic properties in bulk solutions (for example, their activity coefficients at different concentrations) (Robinson and Stokes, 1959).

The exception is lithium, which is hardly surprising, given the special properties of lithium ion in bulk solution. The activity coefficients for K^+, Na^+, Rb^+, Cs^+ vary monotonically with concentration, but the activity coefficient for Li^+ is a nonmonotonic function of the ionic concentration. The activity coefficient for Na^+ is also a nonmonotonic function of the ionic concentration, but the minimum in activity coefficient is not as pronounced as that of lithium ions. We discuss the different properties of Li^+ in the next section, where we show that its special properties can easily be explained if the "excess chemical potential" arose from the difference between the hydration energy and the salvation energy of an ion in the pore of the channel. Once the special properties of Li^+ and Na^+ are dealt with, we find that PNP can fit the *I-V* data from all of the monovalent alkali metals in mixed solutions (including bi-ionic solutions, with different species on the two sides of the ions) with the same parameters already found to fit the data in solutions containing one kind of salt (with small exceptions; see Figs. 12 *C* and 13).

Binary solutions: mixtures of alkali metal salts

In this section, we attempt to describe different chemical interactions of alkali metal cations with the channel. We include the special chemical properties of ions in PNP in the

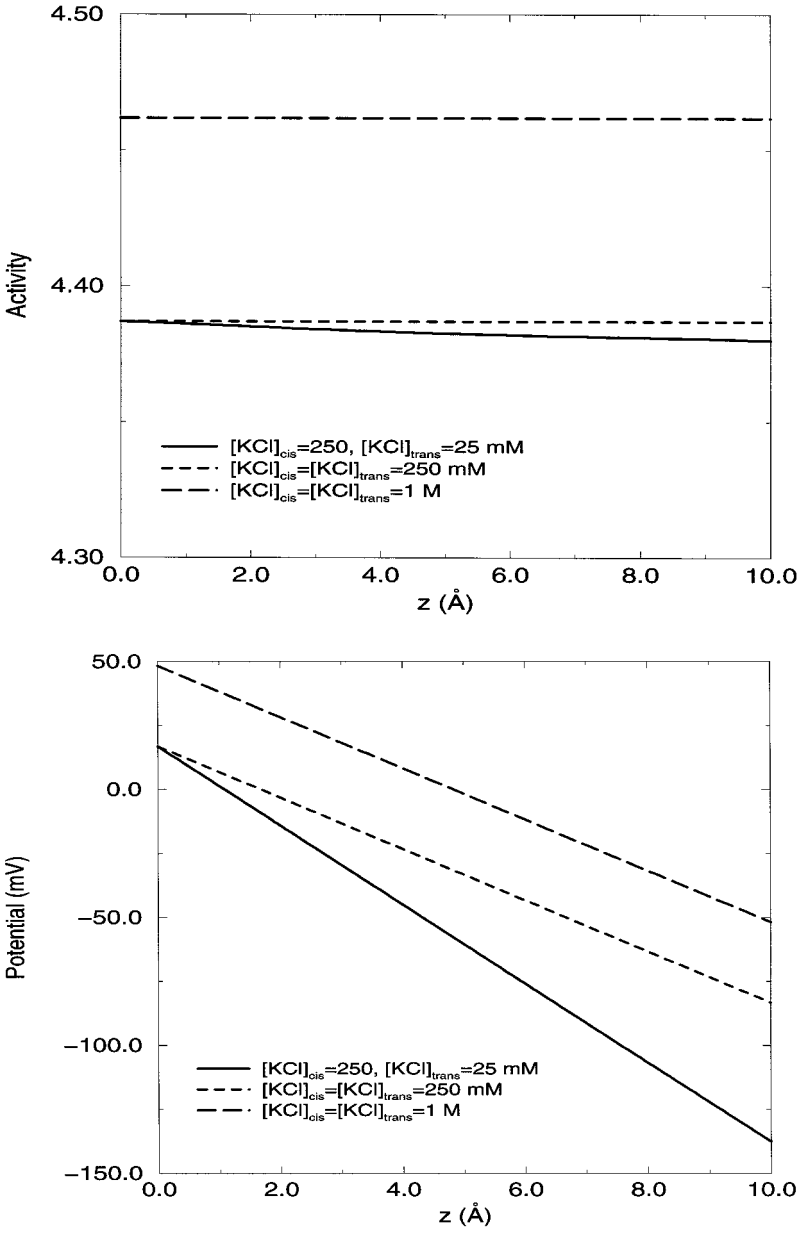

FIGURE 7 (*A*) The activity profiles of the main permeating ions (potassium ions) in solutions of 250(*cis*)‖25(*trans*) mM, symmetrical 250 mM, and symmetrical 1 M, at an applied transmembrane voltage of 100 mV. The portions of the profiles in the baths are omitted. The profiles for chloride ions are also omitted because they are negligible. The solid line is for 250‖25 mM KCl solution, the dashed line is for 250 mM symmetrical salt, and the long-dashed line is for symmetrical 1 M KCl. The profiles show nearly constant occupancy of potassium ions, despite the change of solutions in the bath. However, the electrical potential profiles are very different, as shown in *B*. (*B*) The electrical potential profiles at an applied transmembrane voltage of 100 mV, for different KCl solutions: 250(*cis*)‖25(*trans*) mM, symmetrical 250 mM, and symmetrical 1 M. The solid line is for 250‖25 mM KCl solution, the dashed line is for 250 mM symmetrical salt, and the long-dashed line is for symmetrical 1 M KCl. The potential at $z = 10$ Å clearly shows the ionic strength-dependent screening effect of the charge at the opening of the channel. The net voltage drop is very different from 250‖25 mM solution to symmetrical 250 mM solution, and the profiles inside the channel are shifted nearly 30 mV from 250 mM symmetrical solution to 1 M solution. The change of the electrical profile greatly affects the conductance, but the ion occupancies in the channel are not changed, as shown in *A*.

simplest possible way, as shown in Materials and Methods by including an offset in the chemical potential that is specific for a particular ion species. We assume that this offset in chemical potential is a constant for a given species, independently of the transmembrane potential, the concentration, and other variables and see if such a simple representation can describe all of the chemically specific interactions of a permeating ion with the CRC channel.

TABLE 2 The comparison of three KCl solutions: 250‖25 mM, symmetrical 250 mM, and 1 M at the applied potential of 100 mV

KCl solution (mM)	γ_{100} (pS)	V_{rev} (mV)	O_{K^+}
250‖25	794	−48	1.0154
250‖250	791	0	1.0164
1000‖1000	933	0	1.0337

γ_{100}, $I_{V=100}/(100 - V_{rev})$. V_{rev}, Reversal potential. O_{K^+}, Occupancy of K^+ ions.

Fig. 8 shows precisely how we include the offset in chemical potential. The offset is zero in the bulk solution, where the chemical difference in the properties of the ions is adequately described by the activity coefficients already used in our calculations.

The definition of the regions of the pore—where the chemical potential can take a value different from that in bulk—is somewhat arbitrary, but fortunately our results are nearly the same for different choices. Specifically, if we define the pore proper as the region from 1 Å to 9 Å, we estimate the offset in chemical potential for lithium ions to be −38 mV (the *dashed line*), whereas if the transition from bulk to the pore is made much steeper, by defining the pore

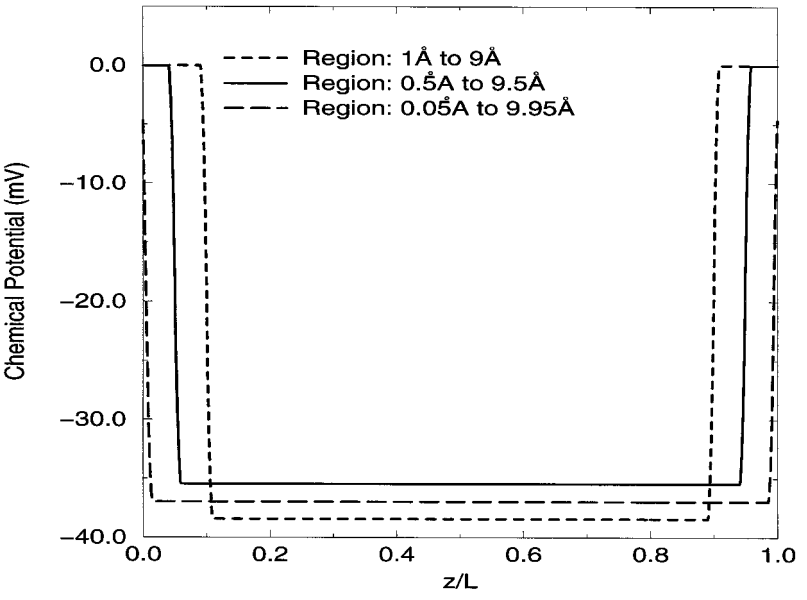

FIGURE 8 The profiles of chemical potential for lithium ions for different choices of transition widths from bulk into the channel pore. The dashed line is for a width of 1 Å, that is, the region of the pore assigned a different chemical potential is then from 1 Å to 9 Å. The solid line is for the region from 0.5 Å to 9.5 Å, and the long-dashed line is for the region from 0.05 to 9.95 Å. All three choices give an estimate of chemical potential near −37 mV.

as the region from 0.05 Å to 9.95 Å, the estimated offset becomes −37 mV (the *long-dashed line*). Similar calculations were made in many cases, and the numerical estimates cluster around −37 mV but do not vary in a physically meaningful way, as far as we can tell. For the remainder of this section, the pore region is supposed to extend from 0.05 Å to 9.95 Å.

We have performed measurements with five different mixed solutions, the solutions being the same on both sides of the channel, namely, in [250 mM LiCl ‖250 mM LiCl], which we call 0% KCl, in [225 mM LiCl‖25 mM KCl], which we call 10% KCl, and in the corresponding 50% KCl, 90% KCl, and 100% KCl, solutions. The protocol is similar to that used in typical mole fraction experiments on biological (Eisenman et al., 1986) or crystalline channels (Isard, 1969).

Fitting Eq. 2 to the entire data set, including the above mole fraction experiments, we obtain an offset in chemical potential for lithium ion $\bar{\mu}(\mathrm{Li}) = -37$ mV, a diffusion coefficient $D(\mathrm{Li}) = 2.253 \times 10^{-7}$ cm^2/s, and the same fixed charge of −4.38 M. Fig. 9 *A* plots the measured conductance versus the mole fraction. The filled circles in Fig. 9 *A* are the points of measured conductances, and the dashed line is there just to connect the points and to show the nonlinear effect visually. Our experiments show a slightly nonlinear dependence of conductance versus the mole fraction, i.e., a mole fraction effect, but there is no minimum, and so no anomalous mole fraction effect is seen. Our fit to the entire current-voltage relations in symmetrical solutions of mixtures LiCl and KCl is shown in Fig. 9 *B*. This is a far more extensive data set than that of simply the conductance, which it includes, of course.

The open circles in Fig. 9 *B* are taken in the 90% KCl solution, and the solid line shows the best fitting theory curve. The open squares are taken in the 50% mixture of KCl and LiCl; the corresponding best fit is the dashed line. The open triangles show the experiment in 10% KCl; the corresponding best fit is the dotted dashed line. Results in the pure KCl and pure LiCl solutions were shown in figures in Chen et al. (1997b) and Fig. 2 *A*, respectively.

The occupancies of permeating ions are shown in Fig. 9 *C*. But the occupancy of chloride ions is low, and we omit them here. The solid line in Fig. 9 *C* is the profile of potassium ions, and the dashed line is the profile for lithium ions when there is no chemical interaction of lithium ions, i.e., when $\bar{\mu}(\mathrm{Li}) = 0$. Because we have symmetrical solutions in a typical mole fraction experiment, we have two flat lines (no diffusion due to no concentration gradients, and the applied voltage is also zero). The calculated conductance based on these profiles is a linear function of mole fraction, and so the usual conductance–mole fraction curve is linear. When there is a chemical interaction of lithium ions, we move the chemical interaction region to 1–9 Å to show the effect clearly in the graph. The solid line with triangles is the profile of potassium ions, and the dashed line with open circles is the profile of lithium ions. The curves show that the chemical interaction of lithium ions repels the nearby potassium ions of higher permeability, making a nonlinear mole fraction plot. Note that $D_{K^+}/D_{Li^+} = 4$ (see Table 3).

With this additional chemical potential, the fit to the current-voltage relation for a solution containing only LiCl salt is greatly improved, especially for the *I-V*'s in Fig. 2 *B*. We plot the new fit in Fig. 10. The open squares in Fig. 10 are the experimental points for 250 mM‖1 M solution, the open circles are for 1 M‖100 mM, and the dashed line and the solid line are the PNP fit, respectively. The fit to other current-voltage relations at different salt concentrations are nearly identical to those in Figs. 2–5, and so we need not repeat them. The improvement is dramatic if we measure the error of the fit to the current-voltage relations in four LiCl solutions alone: the rms of the fit 1.19 pA with and

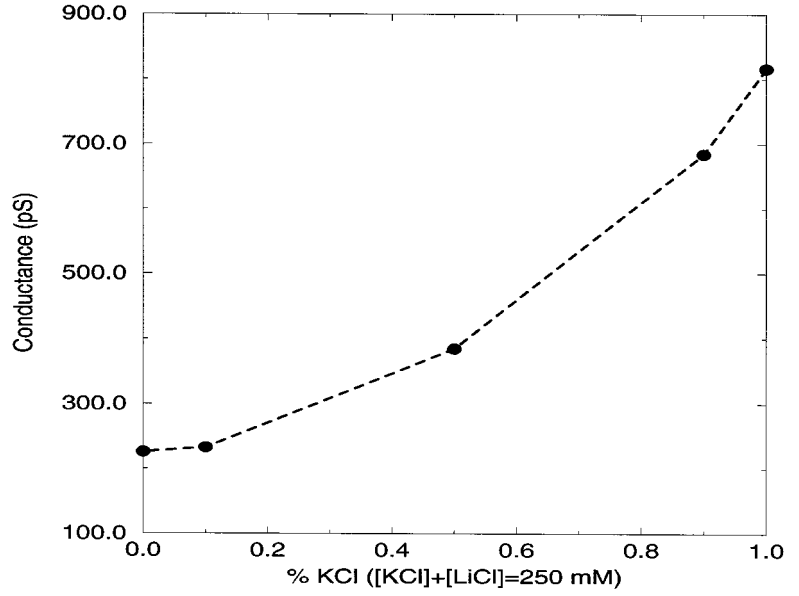

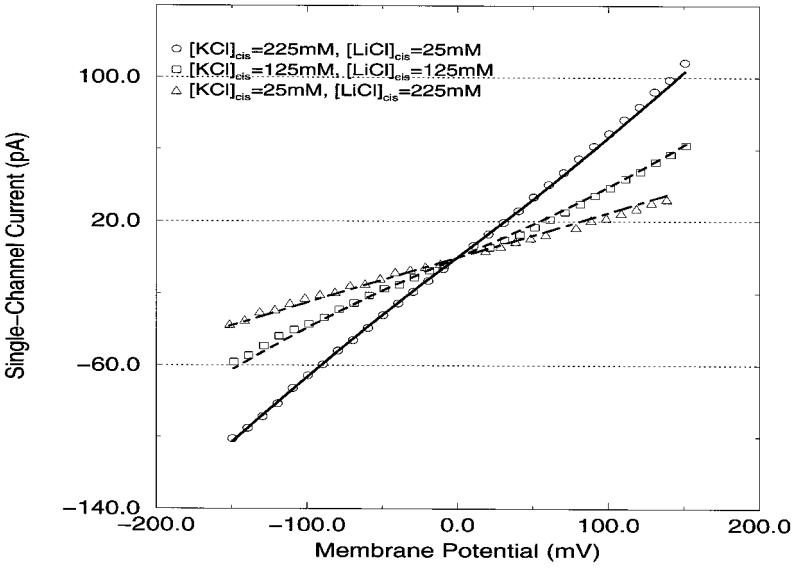

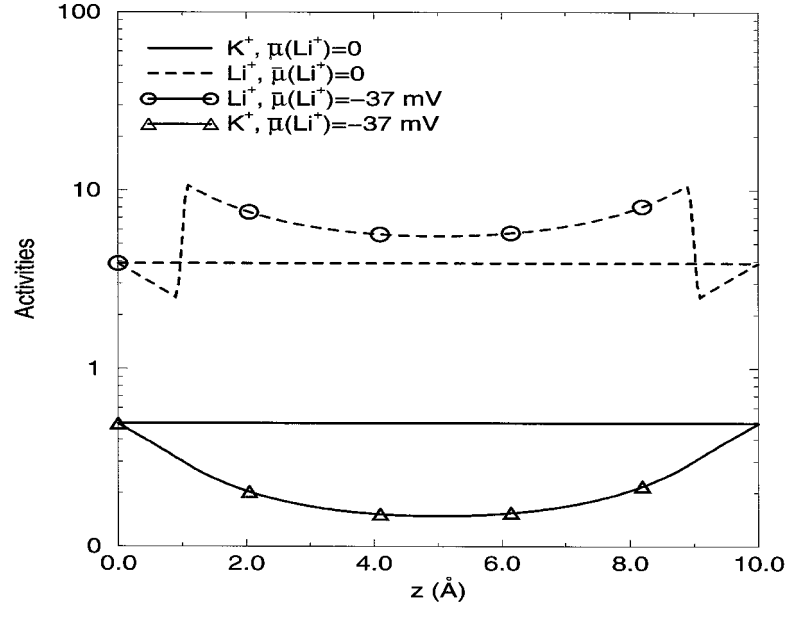

FIGURE 9 (*A*) The mole fraction plot of conductance of CRC of a mixture of KCl and LiCl at a total of 250 mM concentration. The filled circles are the experimental measurement of points of conductance. The dashed line is there just to connect the points. We have found a slight nonlinear mole fraction effect, but no anomalous mole fraction effect. (*B*) The predicted *I-V*'s for mixtures of lithium chloride and potassium chloride at a total ionic concentration of 250 mM. The three *I-V*'s shown here correspond to potassium mole fractions of 10%, 50%, and 90%. The points are the experimental dots, and lines are PNP predictions. The open circles are for 90% K, open squares are for 50% K, and open triangles are for 10% K. The *I-V*'s for pure LiCl are shown in Figs. 2 *A*, and 10. (C) The activities of lithium ions (90%) and potassium ions (10%) at a total of 250 mM along the CRC channel with and without the chemical binding of lithium ions. The part of the profiles in the baths is omitted. The occupancy of chloride ions is so low that it is omitted. The solid line is the profile of potassium ions, and the dashed line is the profile for lithium ions when there is no binding for lithium ions. Because symmetrical solutions are used in a typical mole fraction experiment, the corresponding concentration profiles are flat lines. Two flat lines will give a linear conductance versus mole fraction curve. The solid line with triangles is the profile of potassium ions, when there is a binding of lithium ions, and the dashed line with open circles is the profile of lithium ions. (Note that on the graph we have moved the binding region at 1–9 Å to show the effect clearly.) The curves show that the bound lithium ions repel the potassium ions, making a nonlinear mole fraction plot.

TABLE 3 The summary of cation properties in CRC

Cation	γ (pS)	D_{bulk}	D_{X^+} (10^{-5} cm^2/s)	$\bar{\mu}$ (mV)	$\gamma_{X^+}/\gamma_{K^+}$	D_{X^+}/D_{K^+}	P_{X^+}/P_{K^+}	P_{X^+}/P_{K^+} (Lindsay et al., 1991)
Li^+	205 ± 7 (3)	1.03	0.032 ± 0.005	−37	0.25	0.25	1	0.99
Na^+	502 ± 2 (3)	1.33	0.078 ± 0.009	−25	0.62	0.62	1	1.15
K^+	812 ± 17 (4)	1.96	0.13 ± 0.02	0	1	1	1	1
Rb^+	716 ± 4 (3)	2.07	0.11 ± 0.02	+0.9	0.88	0.88	0.83	0.87
Cs^+	541 ± 2 (3)	2.06	0.083 ± 0.008	+1.2	0.67	0.66	0.69	0.61

γ, Measured conductance at 250 mM symmetrical solutions, with the standard error and number of measurements in parentheses. D_{bulk}, Diffusion coefficient in bulk solutions. D_{X^+}, Diffusion coefficient of cation X^+ in CRC channel estimated by PNP, with error given. $\bar{\mu}$, Excess chemical potential in CRC channel.

4.15 pA without the chemical potential. However, the rms of the fit to all current-voltage relations does not show as large a quantitative improvement, because LiCl salt has a low conductance; hence they are weighted less in the least-squares fit. If the measure defined in Eq. 9 is used, $\delta_{rms}^{scaled} = 2.9\%$. This is a substantial improvement from the previous $\delta_{rms}^{scaled} = 4.3\%$ when $\bar{\mu}(Li) = 0$ mV.

Biionic conditions

Finally, we examine the current-voltage relation in biionic solutions, in particular, the solution of 250 mM KCl *cis* with 250 mM LiCl *trans*, and the mirror image experiment (250 mM LiCl *cis* with 250 mM KCl *trans*, and the *trans* side is electrically grounded; data not shown). The experiment in biionic solutions is designed to estimate the selectivity of a channel by measuring the reversal potential, from which the permeability ratio is conventionally extracted by the Goldman-Hodgkin-Katz equation. However, the *I-V* for biionic KCl and LiCl solution gives a reversal close to 0 mV, which in turn gives a permeability ratio of 1! That is to say, equation 1-13 of Hille (1992) gives $P(K)/P(Li) = 1$; traditional analysis states that the CRC is not selective among potassium and lithium ions, whereas potassium ions are nearly four times more diffusible (or "permeable," because $P_j = D_j/d$, when the partition coefficient is 1, as is conventionally chosen) than lithium ions ($D_{K^+}/D_{Li^+} = 4$; see Table 3), based on the conductance ratio at symmetrical 250 mM solutions.

Fig. 11 *A* shows that PNP fits the *I-V* for the biionic condition well, especially the reversal potential, using the same parameters as in the other solutions. The open circles are the experiment in the biionic condition of 250 mM KCl at the *cis* bath and 250 mM LiCl at the *trans* bath. The solid line is the extended PNP fit, which goes right through the reversal potential of the experiment. The dashed line in the same graph is the one predicted by PNP when $\bar{\mu}(Li) = 0$.

The effect of the chemical interaction of lithium ions in biionic conditions is explained in the next figure (Fig. 11 *B*), where we show how a selective channel seems to give a permeability ratio of 1. In Fig. 11 *B*, the solid line is the activity profile of potassium ions, showing simple diffusion: a linear concentration profile with a constant gradient from the *cis* side (left-hand side) to zero concentration on the *trans* side (right-hand side). The dashed line is the activity profile of lithium ions, again a case of simple diffusion, as we have derived under the condition of high ionic strength for the case without fixed charge (Chen and Eisenberg,

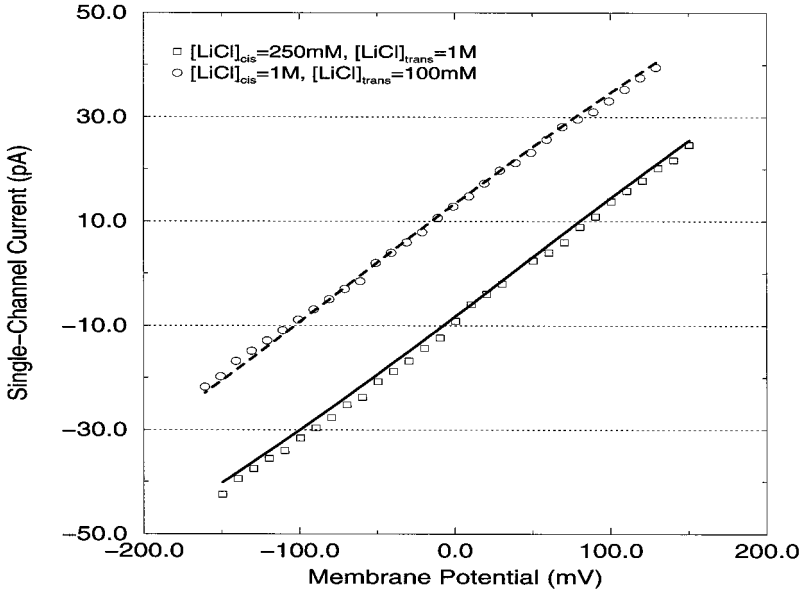

FIGURE 10 The new fit of *I-V*'s for lithium chloride at 250 mM‖1 M and 1 M‖100 mM solutions with the extended PNP formulation with local chemical potential. The open squares are the experimental points for a 250 mM‖1 M solution, and the open circles are for 1 M‖100 mM. The solid line and the dashed line are, respectively, the PNP fits. The chemical potential in the pore for lithium is $\bar{\mu}(Li) = -37$ mV, and a diffusion coefficient of $D(Li) = 2.3 \times 10^{-7}$ cm^2/s. The new fit is significantly improved as compared to the lower panel in Fig. 2 *B*.

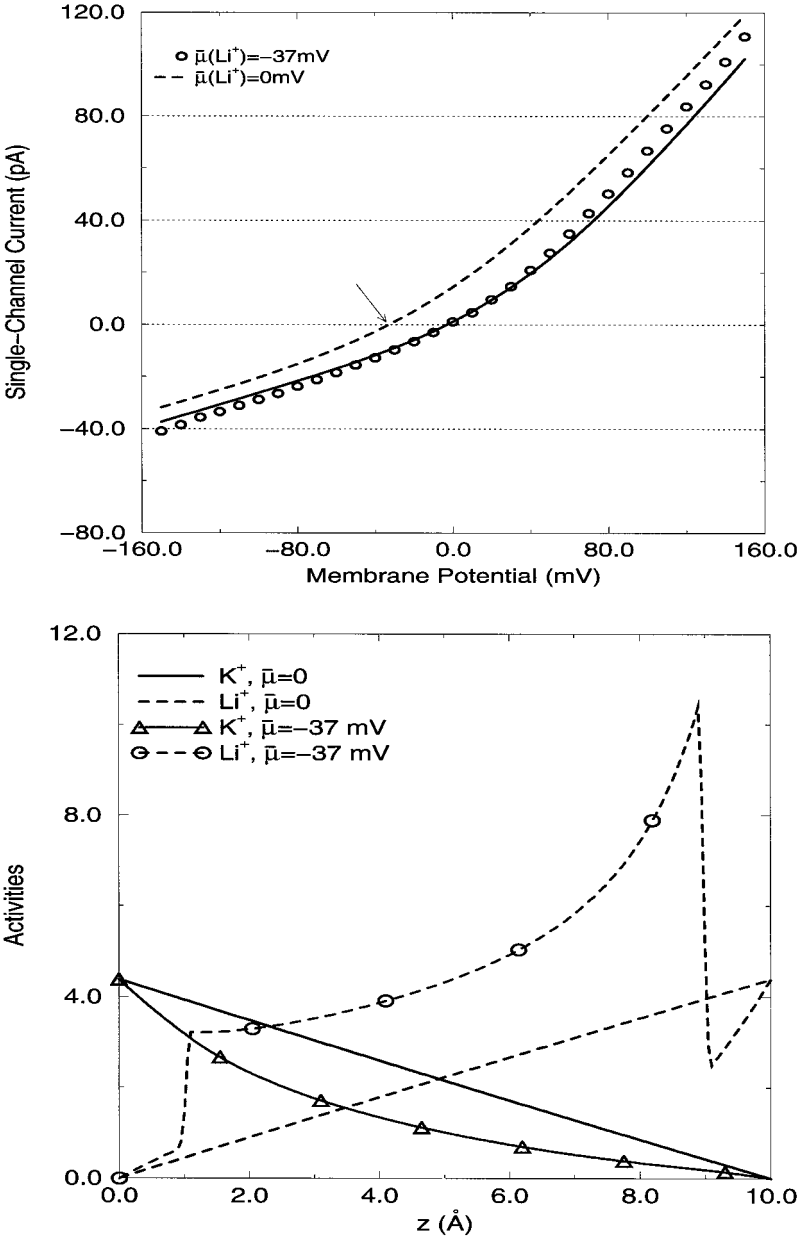

FIGURE 11 (*A*) The predicted *I-V*'s for biionic solutions of lithium chloride and potassium chloride at an ionic concentration of 250 mM. The open circles are an experiment involving the biionic condition of 250 mM KCl at the *cis* side and 250 mM LiCl at the *trans* side. The experiment involving LiCl at *cis* and KCl at *trans* is also performed to confirm the measurement of the reversal potential. The two experiments give the same result. The solid line is the PNP fit when $\bar{\mu}(\mathrm{Li}) = -37$ mV, which goes right through the reversal of the experiment. The dashed line is the predicted *I-V* from PNP when $\bar{\mu}(\mathrm{Li}) = 0$ mV. The arrow indicates that the reversal offset from the theory when there is no chemical interaction of lithium ions with CRC. It is necessary to have chemical interaction of lithium ions to fit both conductance data and reversal measurement in biionic conditions, as explained in *B*. (*B*) The activity profiles of lithium ions and potassium ions for the biionic condition of KCl (*cis*) and LiCl (*trans*) at 250 mM concentration, with and without chemical interaction of lithium ions with CRC. The solid line is the activity profile of potassium ions, which shows a linear concentration profile of a constant gradient from the *cis* side (*left-hand side*) to zero concentration on the *trans* side (*right-hand side*). This is a case of simple diffusion from the highly concentrated left-hand to the right-hand side of zero concentration; so is the case for lithium ions (the *dashed line*). However, the situation is quite different when there is chemical interaction described by an "excess" chemical potential of −37 mV. The binding of lithium ions elevates the concentration of lithium ions in the binding region. (Note that on the graph we have moved the binding region at 1–9 Å to show the effect clearly.) We choose the region for graphical clarity. The lithium ions (the *dashed line* with *open circles*) in the elevated region repel the potassium ions and reduce the probability that potassium ions to occupy the same region, where there is a preferred binding of lithium ions. Consequently, the profile of potassium concentration is sublinear (the *solid line* with *open triangles*), which makes the occupancy of potassium ions lower than when there is no lithium ion binding. The occupancy of potassium ions is reduced; hence the potassium ion flux is getting smaller, making the total electric current go through the origin.

1992). The sum of potassium and lithium ion concentrations (i.e., the total mobile charge) is uniform, which is no surprise if the fixed charge in the pore is nearly neutralized by the mobile ions. Because potassium ions have a diffusion coefficient four times of that of lithium ions, we get a current-voltage relation (shown as the *dashed line* in Fig. 11 *A*) that reverses its direction at a negative applied transmembrane potential.

When there is chemical interaction of lithium ions with CRC, the situation is quite different: the profiles are no longer linear! The chemical interaction of lithium ions elevates the concentration of lithium ions in the region with chemical interaction (shown as the *dashed line* with *open circles* in Fig. 11 *B*). The elevated concentration of lithium ions in the region with chemical interaction of lithium ions repels the potassium ions and reduces the probability that potassium ions occupy the same region, where there is preferred chemical interaction of lithium ions (not potassium ions). Consequently, the profile of potassium concentration is sublinear (shown as the *solid line* with *open triangles* in Fig. 11 *B*). The occupancy of potassium ions is much less when there is chemical interaction of lithium ions than when there is no preferred chemical interaction of lithium ions. Moreover, the effect of the decrease in the potassium occupancy on the current-voltage relation is amplified because $D_{K^+}/D_{Li^+} = 4$ (see Table 3), so that the *I-V* shifts and reverses at a zero applied transmembrane potential, yielding an *I-V* fit to the experiment, shown as the solid line in Fig. 11 *A*.

We show the fit to the measurements in other biionic solutions of KCl and LiCl in Fig. 12. In Fig. 12 *A*, the open circles are the *I-V* points measured experimentally in a

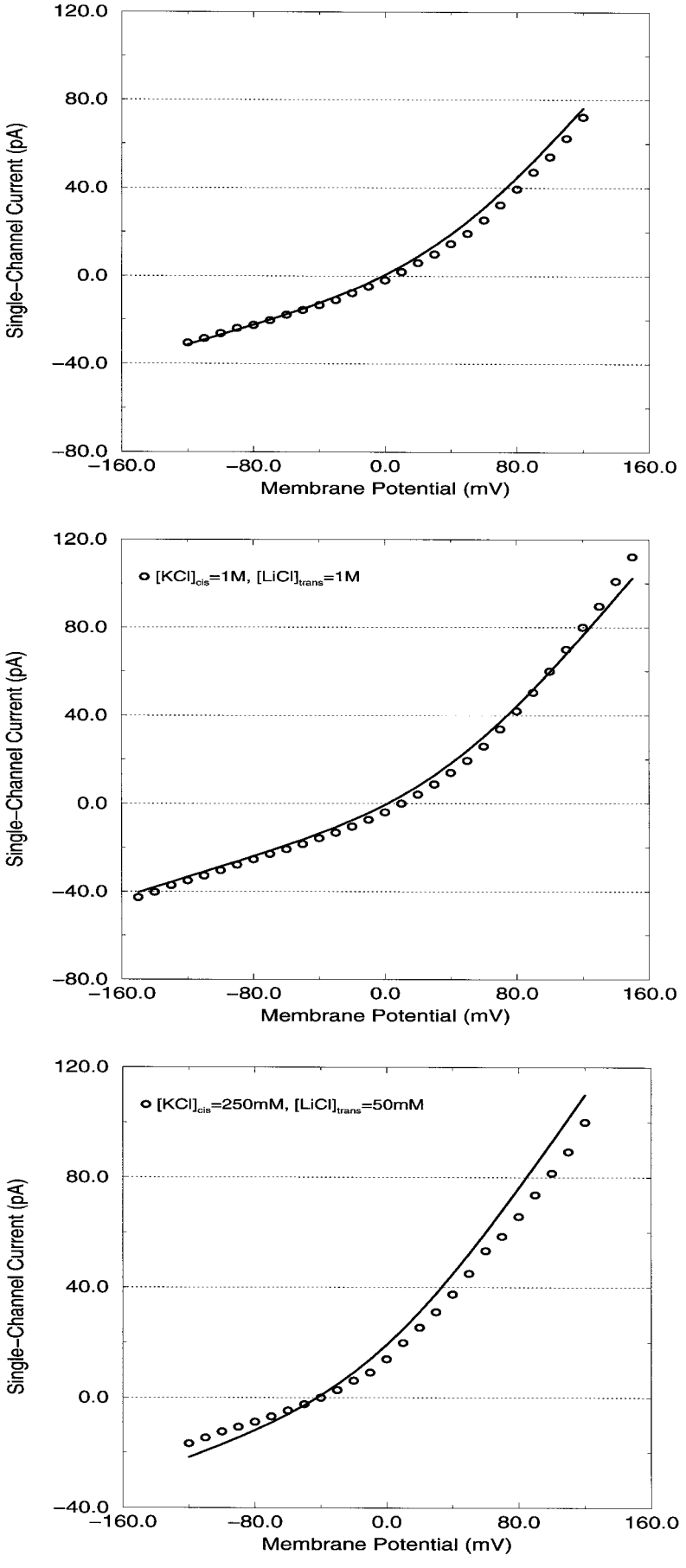

FIGURE 12 (*A*) The fit of the extended PNP to the measured current-voltage relation in the biionic condition of KCl (*cis*) and LiCl (*trans*) at 500 mM concentration when $\bar{\mu}(\mathrm{Li}) = -37$ mV. The open circles are the experimentally measured *I-V* points, and the *solid line* is the PNP fit. (*B*) The fit of the extended PNP to the measured current-voltage relation in the biionic condition of KCl (*cis*) and LiCl (*trans*) at 1 M concentration when $\bar{\mu}(\mathrm{Li}) = -37$ mV. The convention is the same as the one used in *A*. (*C*) The fit of the extended PNP to the measured current-voltage relation in the biionic condition of 250 mM KCl (*cis*) and 50 mM LiCl (*trans*) when $\bar{\mu}(\mathrm{Li}) = -37$ mV. The convention is the same as the one used in *A*.

biionic solution of 500 mM KCl (*cis*) and 500 mM LiCl (*trans*), and the solid line is the fit of the extended PNP. Fig. 12 *B* shows the fit to biionic solution of 1 M KCl (*cis*) and 1 M LiCl (*trans*), and Fig. 12 *C* shows the fit in biionic solution of 250 mM KCl at (*cis*) and 50 mM LiCl at (*trans*). The same convention is used as in Fig. 12 *A*.

We show the fit to the biionic solutions of KCl with NaCl, RbCl, and CsCl in Fig. 13. Fig. 13 *A* shows the fit to the *I-V* in a biionic solution of 250 mM KCl (*cis*) and 250 mM NaCl (*trans*). The open circles are experiment, and the solid line is the extended PNP fit. Once again, the fit is excellent, including at the reversal potential, which is again nearly zero. The fit to the biionic solution of KCl and NaCl gives an excess chemical potential for sodium ions of $\bar{\mu}(\mathrm{Na}) = -25.3$ mV, and $D(\mathrm{Na}) = 5.46 \times 10^{-7}$ cm^2/s. We have refit all current-voltage relations (a total of 40) in the previous section, and we have found that the absolute values of chemical potentials for all other alkali metal ions is less than 2 mV ($\bar{\mu}(\mathrm{K}) = 0$, $\bar{\mu}(\mathrm{Rb}) = 0.94$, $\bar{\mu}(\mathrm{Cs}) = 1.21$ mV). The fits to the current-voltage relation in a solution of biionic KCl and RbCl and biionic KCl and CsCl are shown in Fig. 13, *B* and *C*, respectively. The same convention is used as in Fig. 13 *A*. Even though the fit to the reversal potential in both solutions is good, the fit to the entire *I-V* is not very impressive in the biionic solutions of KCl with RbCl and KCl with CsCl. Further modification of PNP might be needed for these cases.

DISCUSSION

Limitations

The PNP formulation is not without limitations. It is definitely not a TOE (theory of everything). In essence, it is a one-particle mean-field electrodiffusion theory. Ions do interact with each other through the Coulomb force, but it is time averaged Coulombic force in this theory. The averaged probability density distributions (i.e., concentrations; see Barcilon et al., 1993; Eisenberg et al., 1995 for details) contain the averaged interaction captured by the Poisson equation. Theoretically, the validity of PNP theory will be shown if the Nernst-Planck equation can be derived from time-averaged trajectories of interacting single ions, reflecting the discrete nature of ions (Barcilon et al., 1993). Experimentally, the validity of PNP will be shown by its ability to analyze, predict, organize, and motivate experiments. Inputs to the PNP theory are the channel protein charge distribution, the dielectric property of channel and lipid membrane, ion diffusion coefficients, and channel geometry; outputs are physiological observables: the electric current and ionic fluxes. However, PNP does not give the physical basis of diffusion coefficients or dielectric constants. They can only be calculated from the study of the ion motion, including atomic detailed interactions, for example, by molecular dynamics (Roux and Karplus, 1991; Elber et al., 1994; Verkhivker et al., 1992), or even by ab initio quantum mechanical calculations (Zhang et al., 1993; Chen and Callaway, 1992). Our numerical result shows that the chemical interaction of lithium and sodium ions with the CRC pore is different, reflected in the different values of chemical potentials. The details of this local interaction should also be studied at the atomic level by molecular dynamics or at the atomic/electronic level by quantum mechanics.

In the present PNP model, the baths on the two sides of the membrane are not modeled explicitly, but as a boundary condition on the PNP equations. We treat the baths with the simplest two assumptions: 1) thermal equilibrium in the baths; 2) charge neutrality (at a certain location; for details see Chen and Eisenberg, 1993a). We adopt these two assumptions and have derived a unique boundary condition for the present PNP system. The same assumptions are used in theories like Debye-Huckle and Gouy-Chapman (GC).

We are surprised at how good the assumptions are; on the other hand, we are fully aware of the applicability of GC theory to ionic channel systems, which fails even in bulk solutions, especially when divalent ions are present (Henderson, 1983; Lozada-Cassou and Henderson, 1983). Much pioneering work has been carried out to study the geometry effects and to check the applicability of GC theory in ionic channel systems (Dani, 1986; Cai and Jordan, 1990). Those studies are based on the combination of equilibrium Poisson-Boltzmann formulation for the baths and on a kinetic theory (Eyring rate with assumed barriers and wells or the Michaelis-Menten formula for channels of a single-ion occupancy) for the channels to relate the concentration at one specific location to ionic fluxes. These calculations, in principle, include effects of the Stern layer (Cai and Jordan, 1990; Henderson, 1983). However, uniform dielectric constants are used sometimes in these calculations, whereas it is known that the Stern layer has lower dielectric constants than bulk. Therefore, further self-consistent studies including the full details of the channel geometry in three dimensions are necessary to investigate the geometrical effects in biological systems and check the above assumptions against experiment. The future theoretical calculations could be tested with tetramethyloxonium experiments to probe surface charge effects. However, tetramethyloxonium (TMO) is known to do more than just neutralize surface charges (Doyle et al., 1993; Cherbavaz, 1995). It also alters the selectivity of channels, hinting that it binds to the ionic conduction pathway and the selectivity filter.

We have fitted our experiments with different dielectric constants assigned to the pore of the channel. Surprisingly, we have found that there is only a small dielectric effect in CRC. Similar effects have been observed in the Poisson-Boltzmann calculations (Cai and Jordan, 1990). Fig. 7 *B* shows that the electrical potential is a linear profile under various conditions due to the high fixed charge in CRC. The dielectric effect is described by the first term of Eq. 1. A linear electrical potential makes the first term of Eq. 1 zero; therefore there is a small dielectric effect. Another approximation is that we have used uniform dielectric constants in the present calculations, which might overestimate the value

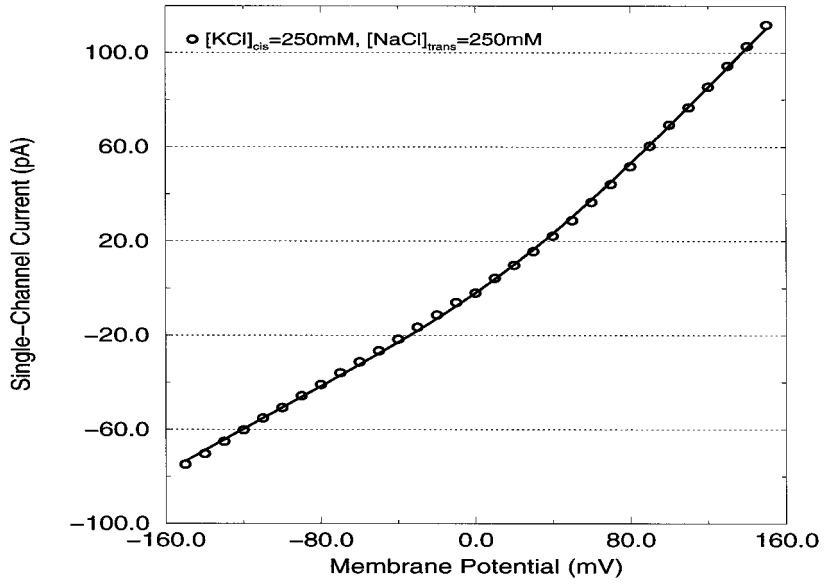

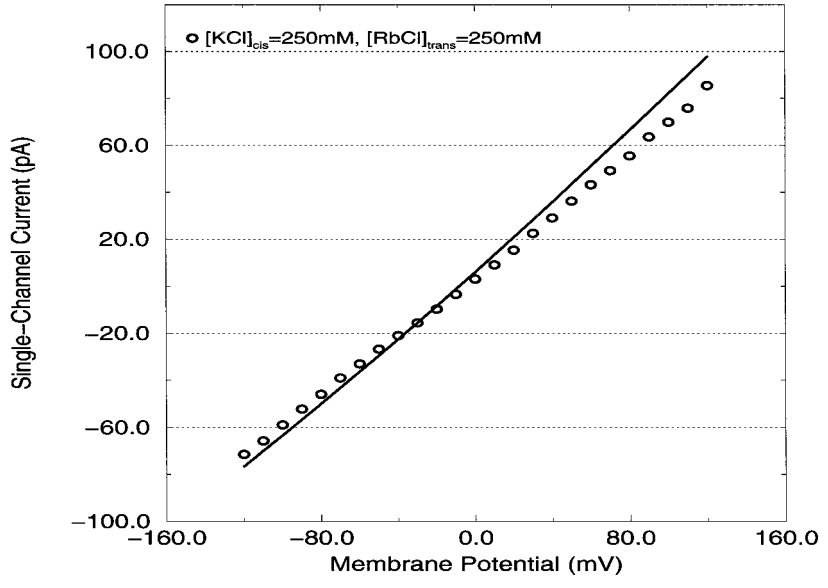

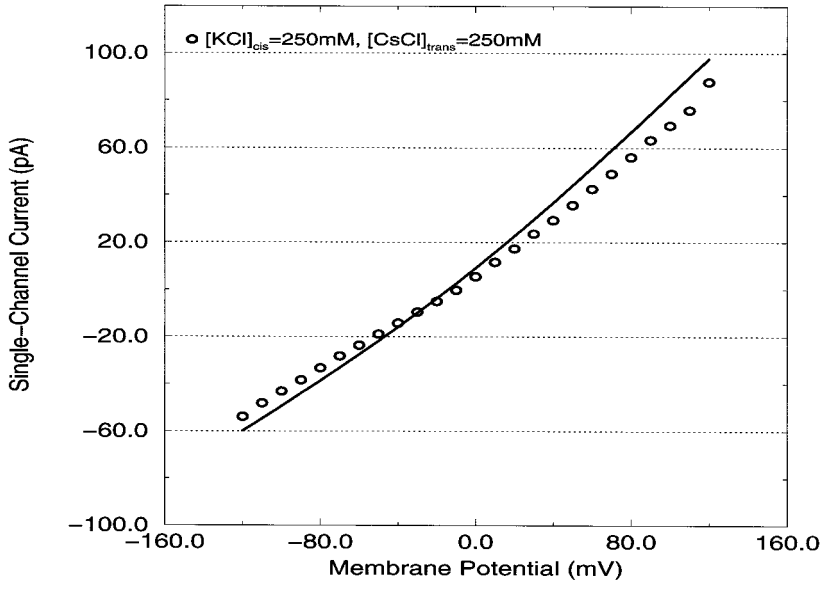

FIGURE 13 (*A*) The fit of the extended PNP to the measured current-voltage relation in the biionic condition of 250 mM KCl (*cis*) and 250 mM NaCl (*trans*) when $\bar{\mu}(\mathrm{Na}) = -25$ mV. The open circles are the experimentally measured *I-V* points, and the solid line is the fit by the extended PNP. (*B*) The fit of the extended PNP to the measured current-voltage relation in the biionic condition of KCl (*cis*) and RbCl (*trans*) at 250 mM concentration when $\bar{\mu}(\mathrm{Rb}) = 0.9$ mV. The convention is the same as the one used in *A*. (*C*) The fit of the extended PNP to the measured current-voltage relation in the biionic condition of 250 mM KCl (*cis*) and 250 mM CsCl (*trans*) when $\bar{\mu}(\mathrm{Cs}) = 1.2$ mV. The convention is the same as the one used in *A*.

of the fixed charge due to the lower value of the dielectric constant in the Stern layer (Henderson, 1983; Lozada-Cassou and Henderson, 1983).

We have also found that it is rather difficult to estimate diffusion coefficients of anions in a cation-selective channel, because the value of diffusion coefficients of anions can hardly change the overall electrical current.

To understand the complexity of ion channel permeation, an extension of PNP is necessary to include important effects other than electrodiffusion. Here we present the first such attempts to include the local chemical potential to formulate the entry/hydration/solvation/exit problem in ion channel permeation. This extension can incorporate the difference in the dehydration energy in bulk solution and hydration by the channel pore (if calculated correctly from some other theory) in the ion permeation steps, just as described in Eisenman's theory.

Selectivity

The permeability ratio and the conductance ratio are two different measures of ion channel selectivity. Permeability ratios measure the competition of different driving forces of fluxes and tell where the concentration gradient driving forces are balanced by the electric potential. Conductance ratios, however, are measures of the relative conduction of ions. In terms of current-voltage relation, the reversal potential tells where the *I-V* reverses its direction, and the conductance tells the slope of the *I-V*. In general, these two measures differ. In particular, this is the case in CRC. The extended PNP, which can include chemical interactions, binding, and hydration energy difference, offers a possible combined treatment. Goldman-Hodgkin-Katz assumes a constant field and it is applicable at best to an oversimplified symmetrical and singly occupied ion channel (Eisenman and Horn, 1983).

Different alkali metal ions interact with the CRC channel differently. This chemical interaction is included in the PNP formulation as an offset of the chemical potential. The offset in the chemical potential is a way of describing the ion-specific chemical interaction with the CRC pore. The offset changes the concentration and activity of the ion species; hence the offset will affect the overall permeation.

To fit the reversal potentials measured in biionic solutions and the conductance measured in solutions of one salt, we need an excess chemical potential of -37 mV for lithium ions and -25 mV for sodium ions. The large value of excess chemical potential for sodium ions ($\sim 1\ k_BT$) surprised us, which also made us revisit table 10 in appendix 8.10 of Robinson and Stokes (1959). We find that there an anomaly in the activity coefficient versus concentration for sodium ions near 1 M concentration. The same anomaly makes lithium ions and sodium ions different from the rest of the alkaline metal ions. This anomaly, of course, is not as pronounced for Na as for lithium ions. It is not enough to justify the value of excess chemical potential of sodium ions we find in CRC, and so the origin of the excess chemical potential for sodium ions must be further investigated.

Here we have used a simple-minded description of the chemical interaction. We have assumed that the chemical interaction of ions with the channel pore is independent of ionic strength and of ion occupancies. Apparently, this is not a very good approximation, as shown by the misfit in Fig. 12 *C*. Even though the fit to the reversal potential is rather accurate, the fit to the entire *I-V* is not that good. It seems that the chemical potential for lithium ions we used is not applicable at ionic strength lower than some 50 mM. Fig. 13, *B* and *C*, shows a different problem with our approximation, here at a single value of chemical potential. In Fig. 13, *B* and *C*, the fit to the reversal potential is rather good; however, the fit to the entire *I-V* (the slope) is not impressive. A good fit in reversal potential shows that the overall net driving force in the biionic solutions of KCl with RbCl and KCl with CsCl is well described in the extended PNP, but its lack of the spatial dependence of chemical potential in the channel pore probably produces the misfit to the rest of the curve.

In the PNP description of ion permeation in CRC, the diffusion coefficients capture the conductance selectivity and almost all aspects of selectivity information, as shown in Fig. 6. The order of the cation diffusion coefficients found in CRC is

$$D(\mathrm{K}) > D(\mathrm{Rb}) > D(\mathrm{Cs}) > D(\mathrm{Na}) > D(\mathrm{Li}), \quad (11)$$

which is indeed the fourth of the famous 11 Eisenman sequences listed in table 6 of Hille (1992). At the low end of the Eisenman sequence, this sequence would have reflected a relatively weak field strength site in that theory. If we calculate the total effective charge distribution on CRC ($\pi r^2 \int P(z)\mathrm{d}z$), we get $-1.02e$, where e is the charge of an electron (absolute value). Being of one charge, the site might be thought to have weak field strength. However, our results show otherwise, i.e., the CRC pore is a strong site: it is equivalent to 4.4 M concentration, and it produces nearly constant occupancy, as shown in Fig. 7 *A*. Our results also show how that chemically preferred interaction (binding) reduces ionic conductance. In CRC, lithium ion conductance is much the lowest among all alkaline metal ions, because of the preferred chemical interaction of lithium ions, in addition to the difference in diffusion coefficients.

We have shown here that the average occupancies are determined self-consistently in PNP. We have shown that the extended PNP can explain the discrepancy between the conductance sequence (measured in a homogeneous ionic solution of one salt) and the permeability sequence (measured in mixtures of salts under biionic condition) discussed in Tinker et al. (1992). In the CRC channel, the conventional definition of selectivity by reversal potential implies that the CRC was not selective, even though the conductance measurement shows selectivity (see Table 3).

Surface charge is the charge at the entrances of the channel in the one-dimensional version of PNP used here,

due to the reduction in the dimensionality. The surface charge, however, should be the charge outside the channel pore in a real three-dimensional system. We (Hollerback, Chen, Nonner, and Eisenberg) are investigating the behavior of the three-dimensional PNP numerically, and we are in the process of comparing the result of the three-dimensional PNP with the one-dimensional PNP used here.

In general, the formula of the reversal potential can be written in a way very similar to the Goldman-Hodgkin-Katz equation as

$$V = \frac{RT}{F} \ln \frac{\sum_{i^+} k'_{i^+} C_{i^+r} + \sum_{i^-} k_{i^-} C_{i^-l}}{\sum_{i^+} k'_{i^+} C_{i^+l} + \sum_{i^-} k_{i^-} C_{i^-r}}, \tag{12}$$

as shown by Patlak some time ago (Patlak, 1960), where l, r denote the left- and right-hand sides, i^+ denotes the monovalent cation species, i^- denotes the monovalent anions, and k's are unidirectional rate constants defined below. The derivation was based on two assumptions: 1) the unidirectional flux ratio obeys the Ussing ratio for each ion species, i.e.,

$$\frac{\overleftarrow{J}_i}{\overrightarrow{J}_i} = \frac{C_{ir}}{C_{il}} e^{-z_i(FV/RT)}, \tag{13}$$

and 2) unidirectional flux is the product of the ionic concentration and the unidirectional rate constants for flux,

$$k_i = \frac{\overleftarrow{J}_i}{C_{ir}}, \tag{14}$$

$$k'_i = \frac{\overrightarrow{J}_i}{C_{il}}. \tag{15}$$

The formula for the reversal potential (Eq. 12) can be generalized to other ratios of flux.

Unidirectional rate constants are the permeabilities only when they are independent of the transmembrane potential and the details of potential profile. Under this condition, the expression of reversal potentials (Eq. 12) reduces to the Goldman-Hodgkin-Katz equation. However, we have shown that unidirectional rate constants depend on the transmembrane potential and the shape of the potential profile. PNP gives (for details of derivation, see Barcilon et al., 1993; Eisenberg et al., 1995; Chen et al., 1997b)

$$k_i = \frac{D_i \pi r^2}{\int_0^d e^{zF\Psi(\zeta)/RT} d\zeta}, \tag{16}$$

$$k'_i = \frac{D_i \pi r^2 e^{zFV/RT}}{\int_0^d e^{zF\Psi(\zeta)/RT} d\zeta}. \tag{17}$$

Saturation

We have shown how conductance saturation can occur by the competition of the entropic effect due to change in ionic concentration with the electrostatic screening caused by the same change in ionic strength. From 250 mM to 1 M symmetrical solutions, the change in ionic strength gives an entropic effect due to concentration difference, as described by exchange rates of ions from bath to channel in Andersen and Procopio (1980) and Andersen and Feldberg (1996). This difference contributes a factor of 3.4 (ratio of activities at 1 M and 250 mM, 0.6040/0.1754) to conductance in favor of the 1 M solution. However, the screening of the surface charge in both baths is different in symmetrical 250 mM and 1 M solutions. The potential in the 1 M solution is 30.25 mV higher than that in the 250 mM solution, because the negative fixed charge at the channel entrances is more screened and produces a more positive potential. A shift in the electrical potential of 30.25 mV is 1.2 k_BT, which is a factor of $e^{1.21} = 3.35$ in favor of the 250 mM solution. The above argument is made quantitatively by the flux formula

$$J_j = D_j \frac{C_L e^{z_j e V_{appl}/k_B T} - C_R}{\int_0^d e^{z_j e \Psi(\xi)/k_B T} d\xi}, \tag{18}$$

derived from Eq. 2 by integration when $\bar{\mu}_j = 0$, where d is the length of the channel. From 250 mM to 1 M, the numerator (both C_L and C_R) in the above formula is increased 3.44 times because of the concentration difference; however, the denominator is also increased 3.35 times because of the shift in the electrical potential of 30.25 mV. The combination of both effects increases the conductance only 18% from 791 pS to 933 pS. This is how the competition of entropy (the supply of ions via bath concentration) with the electrostatic screening of the surface charge at the entrances of the channel produces the saturation effect. Both effects must be analyzed quantitatively, because they act in opposite directions: qualitative or verbal theories do not easily predict the relative sizes of competing effects.

CONCLUSION

We have demonstrated that the selectivity and permeation of monovalent cations in CRC can be studied coherently by the extended PNP. The permeability and conductance of the channel can be understood at all potentials and in all measured solutions. This description unites the chemically specific friction (described by diffusion coefficients), chemically specific short-range interaction (described by excess chemical potentials), and the electrical energy profile for permeation, all described by the extended Nernst-Planck and Poisson equations. This theory forms a systematic and quantitative treatment of selectivity and conduction that unites the equilibrium electrostatic selectivity of the Eisenman theory with the nonequilibrium frictional selectivity of the Goldman-Hodgkin-Katz constant-field theory.

This work is supported in part by National Institutes of Health grants AR18687 and HL27430 to GM, and by DARPA (N65236-98-1-5409) and the National Science Foundation (DBI-9726338) to RSE.

REFERENCES

Andersen, O. S., and S. W. Feldberg. 1996. The heterogeneous collision velocity for hydrated ions in aqueous solutions is similar to 10^4 cm/s. *J. Phys. Chem.* 100:4622–4629.

Andersen, O. S., and J. Procopio. 1980. Ion movement through gramicidin A channels. On the importance of the aqueous diffusion resistance and ion-water interactions. *Acta Physiol. Scand. Suppl.* 481:27–35.

Asther, W. A., J. Yang, and R. W. Tsien. 1994. Structural basis of ion channel permeation and selectivity. *Curr. Opin. Neurobiol.* 4:313–323.

Barcilon, V., D. P. Chen, and R. S. Eisenberg. 1992. Ion flow through narrow membrane channels. Part II. *SIAM J. Appl. Math.* 52:1405–1425.

Barcilon, V., D. P. Chen, R. S. Eisenberg, and M. A. Ratner. 1993. Barrier crossing with concentration boundary conditions in biological channels and chemical reactions. *J. Chem. Phys.* 98:1193–1212.

Berry, R. S., S. A. Rice, and J. Ross. 1980. Physical Chemistry. John Wiley and Sons, New York.

Bezanilla, F., and C. M. Armstrong. 1972. Negative conductance caused by entry of sodium and cesium ions into the potassium channels of squid axons. *J. Gen. Physiol.* 60:588–608.

Cai, M., and P. C. Jordan. 1990. How does vestibule surface charge affect ion conduction and toxin binding in a sodium channel? *Biophys. J.* 57:883–891.

Chen, D. P. 1997. Nonequilibrium thermodynamics of transports in ion channels. *In* Progress of Cell Research: Towards Molecular Biophysics of Ion Channels, Vol. 6 of Progress in Cell Research. M. Sokabe, A. Auerbach, and F. Sigworth, editors. Elsevier Science, Amsterdam. 269–277.

Chen, D. P., and R. S. Eisenberg. 1992. Constant fields and constant gradients in open ionic channels. *Biophys. J.* 61:1372–1393.

Chen, D. P., and R. S. Eisenberg. 1993a. Charges, currents, and potentials in ionic channels of one conformation. *Biophys. J.* 64:1405–1421.

Chen, D. P., and R. S. Eisenberg. 1993b. Flux, coupling, and selectivity in ionic channels of one conformation. *Biophys. J.* 65:727–746.

Chen, D. P., P. Kienker, J. Lear, and B. Eisenberg. 1997a. Permeation through an open channel: Poisson-Nernst-Planck theory of a synthetic channel. *Biophys. J.* 72:97–116.

Chen, D. P., L. Xu, A. Tripathy, G. Meissner, and B. Eisenberg. 1997b. Permeation through the calcium release channel of cardiac muscle. *Biophys. J.* 73:1337–1354.

Chen, H., and J. Callaway. 1992. Lattice dielectric functions based on the shell model. *Phys. Rev. B.* 45:2085–2087.

Cherbavaz, D. B. 1995. Trimethyloxonium modification of batrachotoxin-activated Na channels alters functionally important protein residues. *Biophys. J.* 68:1337–1346.

Coronado, R., J. Morrissette, M. Sukhareva, and D. M. Vaughan. 1994. Structure and function of ryanodine receptors. *Am. J. Physiol.* 266: C1485–C1504.

Dani, J. 1986. Ion-channel entrances influence permeation: net charge, size, shape, and binding considerations. *Biophys. J.* 49:607–618.

Davis, M. E., and J. A. McCammon. 1990. Electrostatics in biomolecular structure. *Chem. Rev.* 90:509–521.

Doyle, D. D., Y. Guo, S. L. Lustig, J. Satin, R. B. Rogart, and H. A. Fozzard. 1993. Divalent cation competition with [^{3}H]saxitoxin binding to tetrodotoxin-resistant and -sensitive sodium channels. *J. Gen. Physiol.* 101:153–182.

Eisenberg, R., M. M. Klosek, and Z. Schuss. 1995. Diffusion as a chemical reaction: stochastic trajectories between fixed concentrations. *J. Chem. Phys.* 102:1767–1780.

Eisenman, G. 1962. Cation selective glass electrodes and their mode of operation. *Biophys. J.* 2:259–323.

Eisenman, G., and R. Horn. 1983. Ionic selectivity revised: the role of kinetic and equilibrium processes in ion permeation through channels. *J. Membr. Biol.* 76:197–225.

Eisenman, G., R. Latorre, and C. Miller. 1986. Multi-ion conduction and selectivity in the high-conductance Ca^{++}-activated K^+ channel form skeletal muscle. *Biophys. J.* 50:1025–1034.

Elber, R., D. P. Chen, D. Rojewska, and R. S. Eisenberg. 1994. Sodium in gramicidin: an example of a permion. *Biophys. J.* 68:906–924.

Forsten, K. E., R. E. Kozack, D. A. Lauffenburger, and S. Subramaniam. 1994. Numerical solution of the nonlinear Poisson-Boltzmann equation for a membrane-electrolyte system. *J. Phys. Chem.* 98:5580–5586.

Goldman, D. E. 1943. Potential, impedance, and rectification in membranes. *J. Gen. Physiol.* 27:37–60.

Green, W. N., and O. S. Andersen. 1991. Surface charges and ion channel function. *Annu. Rev. Physiol.* 53:341–359.

Hänggi, P., P. Talkner, and M. Borokovec. 1990. Reaction-rate theory: fifty years after Kramers. *Rev. Mod. Phys.* 62:251–341.

Henderson, D. 1983. Recent progress in the theory of the electric double layer. *Prog. Surface Sci.* 13:197–224.

Hille, B. 1975. Ionic selectivity of Na and K channels of nerve membranes. *In* Lipid Bilayers and Biological Membranes: Dynamic Properties. Membranes—A Series of Advances. G. Eisenman, editor. Marcel Dekker, New York. 255–323.

Hille, B. 1992. Ionic Channels of Excitable Membranes, 2nd Ed. Sinauer Associates, Sunderland, MA.

Hille, B., and W. Schwarz. 1978. Potassium channels as multi-ion single-file pores. *J. Gen. Physiol.* 72:409–442.

Hodgkin, A. L., and B. Katz. 1949. The effect of sodium ions on the electrical activity of the giant axon of the squid. *J. Gen. Physiol.* 108:37–77.

Honig, B., and A. Nichols. 1995. Classical electrostatics in biology and chemistry. *Science.* 268:1144–1149.

Isard, J. O. 1969. The mixed alkali effect in glass. *J. Non-Crystalline Solids.* 1:235–261.

Jordan, P. C. 1982. Electrostatic modeling of ion pores, energy barriers and electric field profiles. *Biophys. J.* 39:157–164.

Lindsay, A. R. G., S. D. Manning, and A. J. Williams. 1991. Monovalent cation conductance in the ryanodine receptor-channel of sheep cardiac muscle sarcoplasmic reticulum. *J. Physiol. (Lond.).* 439:463–480.

Lozada-Cassou, M., and D. Henderson. 1983. Application of the hypernetted chain approximation to the electrical double layer: comparison with Monte Carlo results for 2:1 and 1:2 salts. *J. Phys. Chem.* 87: 2821–2824.

Meissner, G. 1986. Ryanodine activation and inhibition of the Ca^{2+} release channel of sarcoplasmic reticulum. *J. Biol. Chem.* 261:6300–6306.

Meissner, G. 1994. Ryanodine receptor Ca^{2+} release channels and their regulation by endogenous effectors. *Annu. Rev. Physiol.* 56:485–508.

Neyton, J., and C. Miller. 1988. Potassium blocks barium permeation through a calcium-activated potassium channel. *J. Gen. Physiol.* 92: 549–567.

Nonner, W., D. P. Chen, and B. Eisenberg. 1998. Anomalous mole fraction effect, electrostatics, and binding in ionic channels. *Biophys. J.* 74: 2327–2334.

Parsegian, A. 1969. Energy of an ion crossing a low dielectric membrane: solutions to four relevant electrostatic problems. *Nature.* 221:844–846.

Patlak, C. 1960. Derivation of an equation for the diffusion potential. *Nature.* 188:944–945.

Press, W. H., S. A. Teukolsky, W. T. Vetterling, and B. P. Flannery. 1992. Numerical Recipes: the Art of Scientific Computing, 2nd Ed. Cambridge University Press, New York.

Reuter, H., and C. F. Stevens. 1981. *J. Membr. Biol.* 57:103–118.

Robinson, R. A., and R. H. Stokes. 1959. Electrolyte Solutions, 2nd Ed. Butterworths, London.

Roux, B., and M. Karplus. 1991. Ion transport in a model gramicidin channel: structure and thermodynamics. *Biophys. J.* 59:961–981.

Selberherr, S. 1984. Analysis and Simulation of Semiconductor Devices. Springer-Verlag, Vienna and New York.

Simon, W., and W. E. Morf. 1973. *In* Membranes. A Series of Advances. G. Eisenman, editor. Marcel Dekker, New York. 329–375.

Smith, J., T. Imagawa, J. Ma, M. Fill, K. Campbell, and R. Coronado. 1988. Purified ryanodine receptor from rabbit skeletal muscle is the calcium-release channel of sarcoplasmic reticulum. *J. Gen. Physiol.* 92:1–26.

Tinker, A., A. R. G. Linday, and A. J. Williams. 1992. A model for ionic conductance in the ryanodine receptor channel of sheep cardiac muscle sarcoplasmic reticulum. *J. Gen. Physiol.* 100:495–517.

Tinker, A., and A. Williams. 1995. Measuring the length of the pore of the sheep cardiac sarcoplasmic reticulum calcium-release channel using related trimethylammonium ions as molecular calipers. *Biophys. J.* 68: 111–120.

Tu, Q., P. Velez, M. Brodwick, and M. Fill. 1994. Streaming potentials reveal a short ryanodine-sensitive selectivity filter in cardiac Ca^{2+} release channel. *Biophys. J.* 67:2280–2285.

Van Huffel, S., and J. Vandewalle. 1991. The Total Least Squares Problem: Computational Aspects and Analysis, Vol. 9 of Frontier in Applied Mathematics. Society for Industrial and Applied Mathematics, Philadelphia.

Verkhivker, G., R. Elber, and Q. H. Gibson. 1992. Microscopic modeling of ligand diffusion through the protein leghemoglobin: computer simulations and experiments. *J. Am. Chem. Soc.* 114:7866–7878.

Williams, A. 1992. Ionic conduction and discrimination in the sarcoplasmic reticulum ryanodine receptor/calcium release channel. *J. Muscle Res. Cell Motil.* 13:7–26.

Zhang, Z., H. Chen, B. C. Bolding, and M. Lagally. 1993. Vacancy diffusion on si(100)-2x1. *Phys. Rev. Lett.* 71:3677–3680.